Business Code :	1-10-INC-2200	Market or Order Number :	DV22AGR001: Product DV22AGR002: Services
		Classification :	Internal distribution

Internal Distribution: Project Team

External Distribution: Customer INCAS

Written by	Verified by	Approved by	Approved by
O. CLAUZIER **RF Engineer** Visa OLIVIER CLAUZIER Signature numérique de OLIVIER CLAUZIER Date : 2023.06.26 18:20:07 +02'00'	**J. AUCOURT** **Technical Project Manager** Visa	Visa	Visa

Pages Number: 40

3D Electromagnetic simulation analysis FH-INCAS aircraft

EVOLUTIONS

IND.	DATE	SECR.	WRITER	OBJECT
00	30/05/23		O. CLAUZIER	Initial version

SUMMARY

TABLES OF FIGURES

APPLICABLE DOCUMENTS

Rep.	Title	Reference	Indice	Date
A0	Agreement for the supply of FlashHawk product between INCAS and AVANTIX	DV22AGR001	N/A	22/11/2022
A1	Agreement for the supply of services between INCAS and AVANTIX for FlashHawk integration	DV22AGR002	N/A	13/12/2022
A2	Technical Proposal FlashHawk Product	DV22PTE037	01	16/11/2022

1. REFERENCE DOCUMENTS

Rep.	Title	Reference	Indice	Date
R0	AVANTIX Quality Manual	96QP007	25	21/11/2019
R1	Interface Control Document (ICD)	DT20ICD001	14	26/05/2023

2. GLOSSARY ABBREVIATIONS

Wording	Definition
AR	Antenna Array
EM	ElectroMagnetic
BBVx	Low band antenna x with vertical polarization
BBHx	Low band antenna x with horizontal polarization
BHxP	High band antenna x with +45° polarization
BHxM	High band antenna x with -45° polarization
SBR	Shooting and Bouncing Rays
RF	Radio Frequency
PDR	Preliminary Design Review
dBi	Decibels with respect to an isotropic radiator
PEC	Perfect Electric Conductor
PMR	Private Mobile Radio
DL	DownLink
DoA	Direction of Arrival
SNR	Signal-to-Noise Ratio

3. INTRODUCTION

This document gives the 3D electromagnetic simulation analysis of the FlashHawk Antenna Array installed on the BN2 Islander aircraft. The electromagnetic simulations were performed by the software HFSS from Ansys. The aims of these simulations are multiple:

- In the first part of the document, we analyze the aircraft influence on the Antenna Array radiation patterns. To begin, this study investigates the potential masking areas due to the presence of the aircraft fuselage on one side of the Antenna Array. Then, an analysis on the localization performances is discussed in order to estimate if a calibration campaign in high band is necessary.

- In the second part of the document, we analyze the coupling between on board emitters and the Antenna Array. The objective is to verify the non-destruction of the AR due to high power emissions. Then, the impact on AR sensitivity is examined.

4. INFLUENCE OF THE INCAS BN2 ISLANDER ON THE AR PERFORMANCES

4.1. AR SIMULATIONS

First of all, the AR is modelized on the HFSS software. Antenna dimensions and the material characteristics are carefully defined conforming to the final product (see figure 1). The HFSS software solves the Maxwell equations thanks to the finite element method (FEM) in the frequency domain.

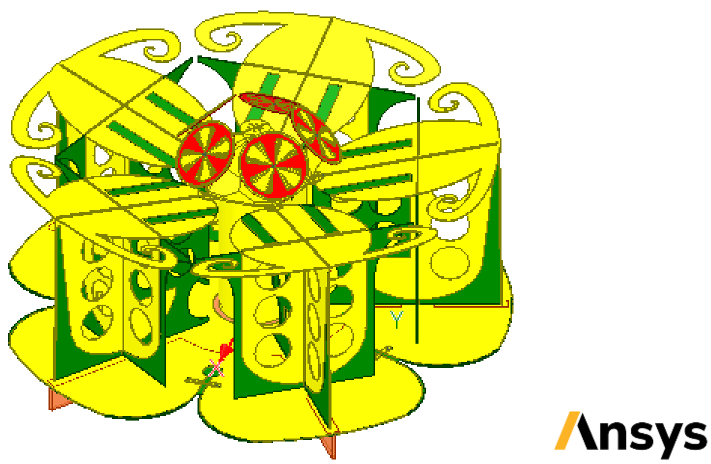

Figure 1: AR design on Ansys HFSS.

4.2. BN2 ISLANDER MODEL

A model of the BN2 Islander has been bought on Hum3D website (https://hum3d.com). The model (see figure 2a.) has 392 solids with many details such as aircraft cockpit. For simulation duration constraints, some simplifications have been realized (see figure 2b.). These simplifications do not modify the aircraft main dimensions. Furthermore, due to the propeller rotation speed, the aircraft helixes have been considered as a cylinder (see figure 2c.). The aircraft is completely defined by PEC (Perfect Electric Conductor) material.

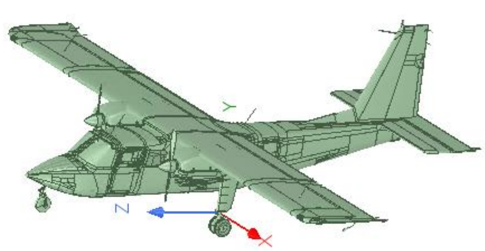	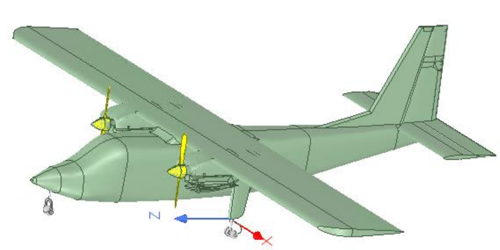
a.	***b.***

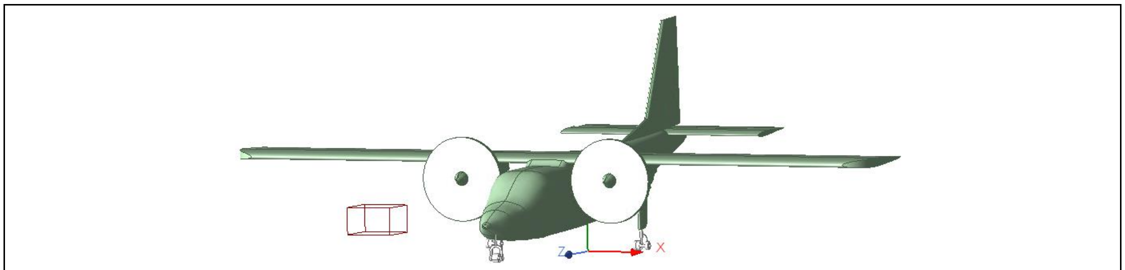

c.

Figure 2: BN2 Islander model. a. Original model from Hum3D website. b. Simplified model. c. Simplified model with cylinders instead of helixes.

The AR position is fixed according to the PDR decisions: the AR is at 50 cm from the ground (see figure 2c. and figure 3). Then, in simulations, the AR performances on the BN2 Islander aircraft are obtained thanks to SBR (Shooting and Bouncing Rays) method.

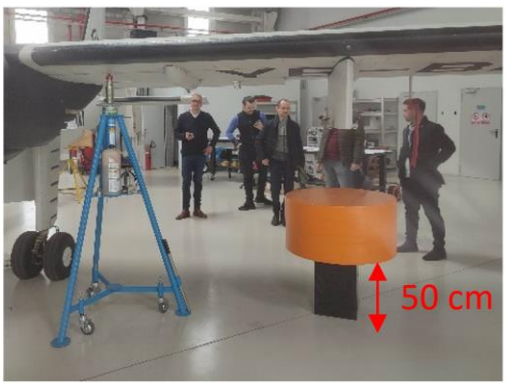

Figure 3: Antenna Array position on INCAS BN2 Islander.

4.3. AR PERFORMANCES ON BN2 ISLANDER AIRCRAFT

As a reminder, the AR is divided in two sub-bands:

- The low band: 30-764 MHz where the AR is calibrated on the aircraft during the calibration campaign,
- The high band: 764-3000 MHz where the AR is calibrated (alone) in an anechoic chamber.

The influence of the aircraft on the AR radiation patterns is separated in two parts following the considered sub-bands.

4.3.1. IN LOW BAND (30-764 MHZ)

To illustrate the influence of the BN2 Islander on the AR radiation patterns, some cartographies at different frequencies (70 MHz, 130 MHz, 420 MHz, 750 MHz) are given in the following figures. The first three frequencies correspond to PMR frequencies. The last one is close to a cellular band (B28).

First, the antennas position in the coordinate system is given in the following figure 4.

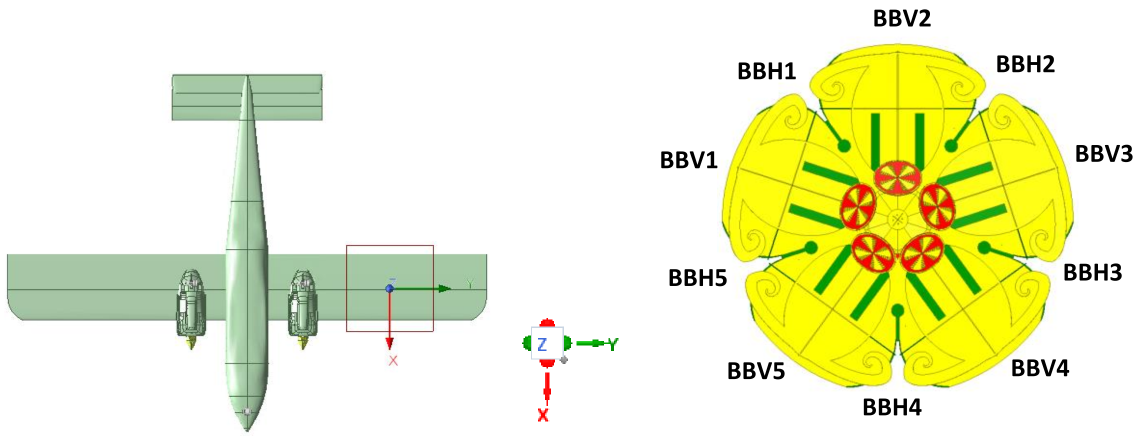

Figure 4: Antennas position in the coordinate system.

4.3.1.1. 70 MHz

The figure 5 plots the BBV1 gain patterns (on E_θ and E_ϕ component) at 70 MHz. The figure compares the gain patterns for two different AR positions on the aircraft:

- AR under the belly (in the two top cartographies),
- AR under the wings (in the two lower cartographies).

As illustrated, for the two components of the E-field, **the gain patterns are drastically different following the AR positions on the aircraft.** Furthermore, at 70 MHz, we can also note **no masking area** due to the aircraft fuselage.

The same observations are valid on the other antennas: BBV2 (see figure 6), BBV3 (see figure 7), BBV4 (see figure 8) and BBV5 (see figure 9).

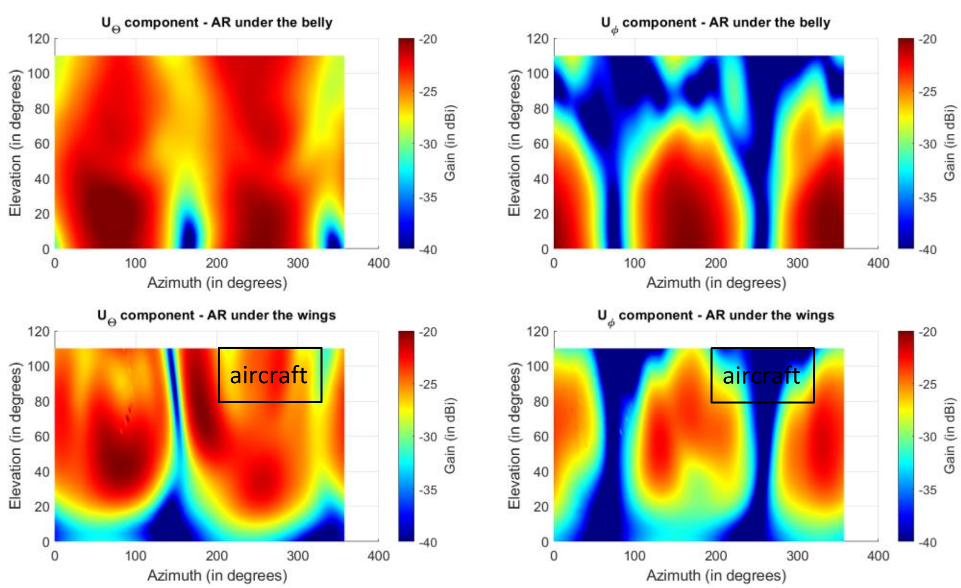

Figure 5: BBV1 gain patterns at 70 MHz. AR under the belly (upper figures); AR under the wings (lower figures).

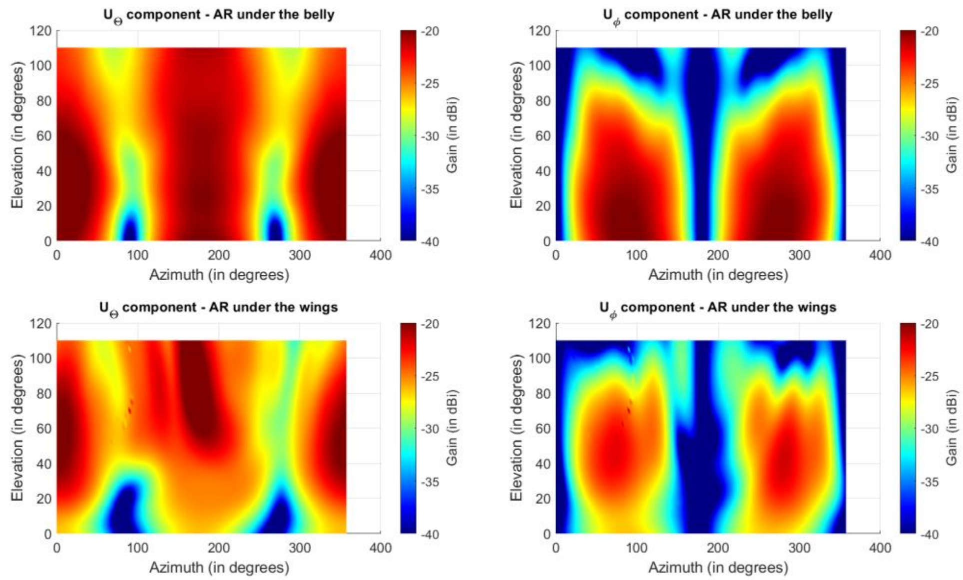

Figure 6: BBV2 gain patterns at 70 MHz. AR under the belly (upper figures); AR under the wings (lower figures).

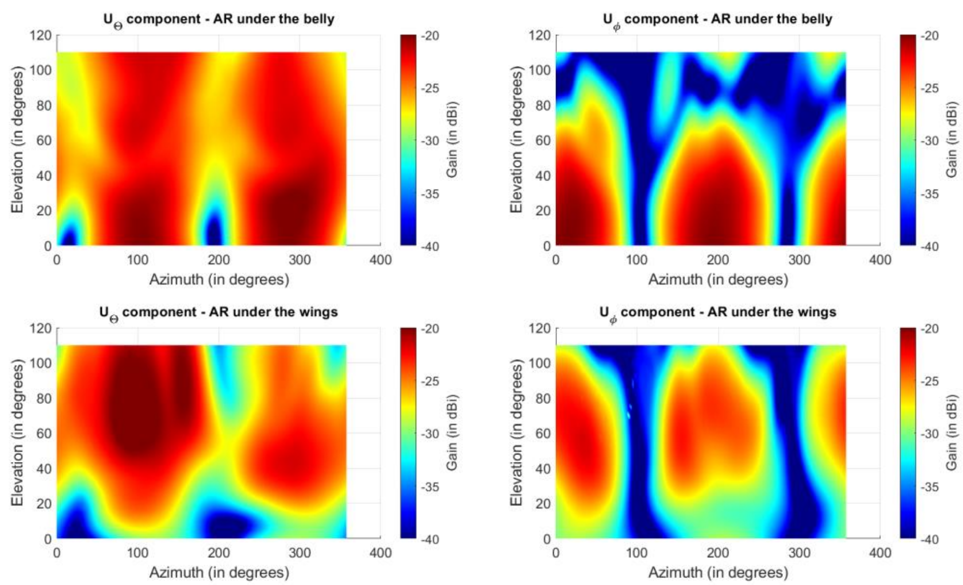

Figure 7: BBV3 gain patterns at 70 MHz. AR under the belly (upper figures); AR under the wings (lower figures).

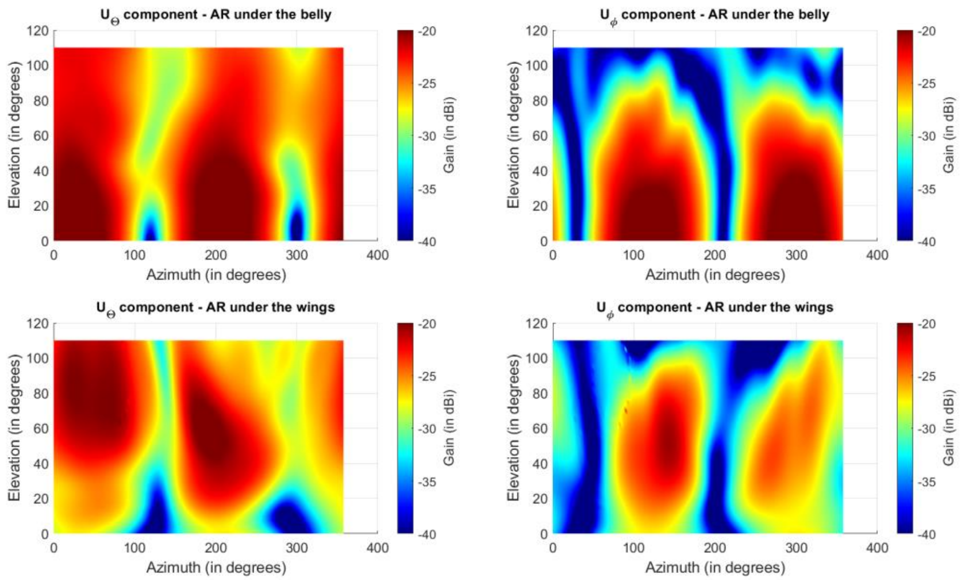

Figure 8: BBV4 gain patterns at 70 MHz. AR under the belly (upper figures); AR under the wings (lower figures).

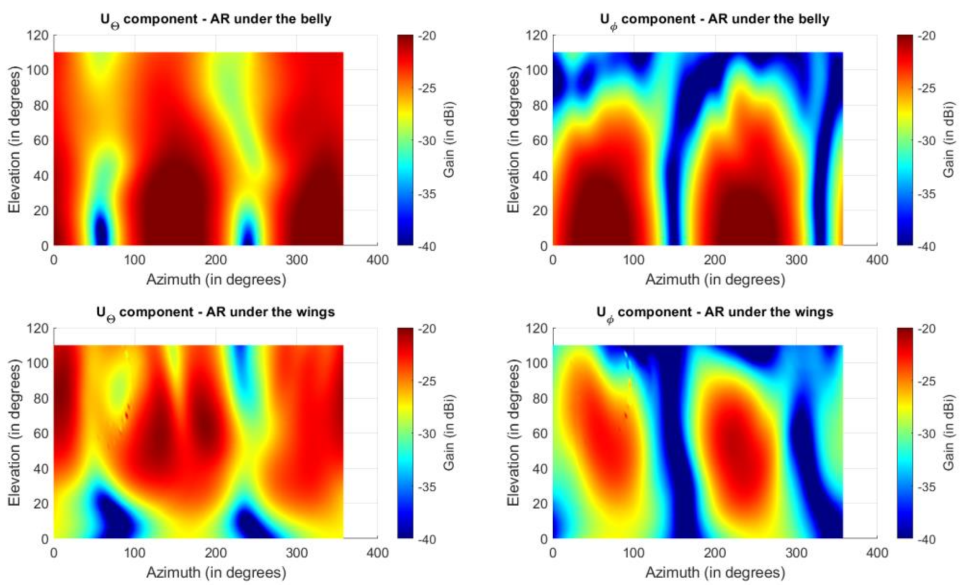

Figure 9: BBV5 gain patterns at 70 MHz. AR under the belly (upper figures); AR under the wings (lower figures).

4.3.1.2. 130 MHz

The figure 10 plots the BBV1 gain patterns (on E_θ and E_ϕ component) at 130 MHz. As previously, **we notice an important difference between gain patterns following the AR positions on the aircraft.** Moreover, we can observe, especially on the E_θ component, a masking area due to the presence of the aircraft fuselage.

The same observations are valid on the other antennas: BBV2 (see figure 11), BBV3 (see figure 12), BBV4 (see figure 13) and BBV5 (see figure 14).

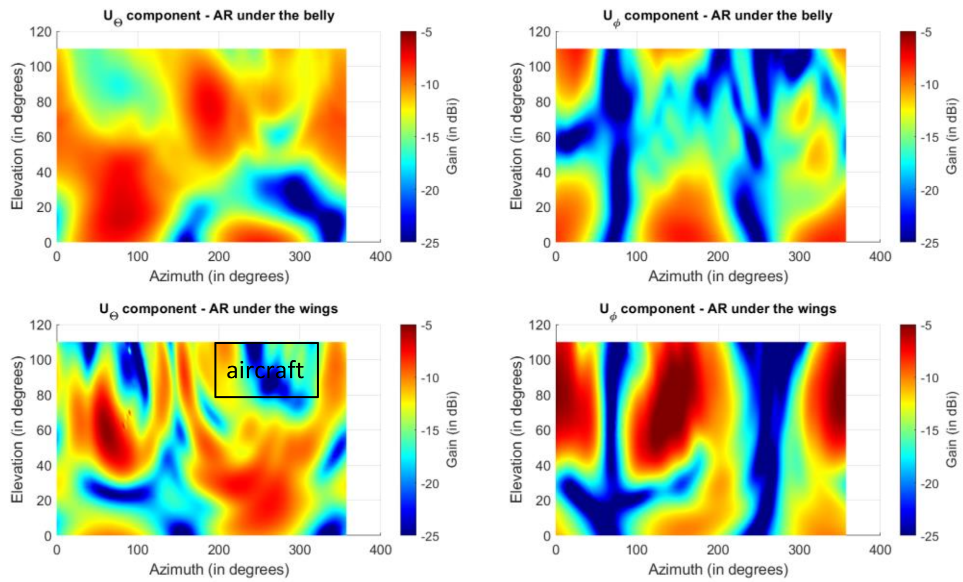

Figure 10: BBV1 gain patterns at 130 MHz. AR under the belly (upper figures); AR under the wings (lower figures).

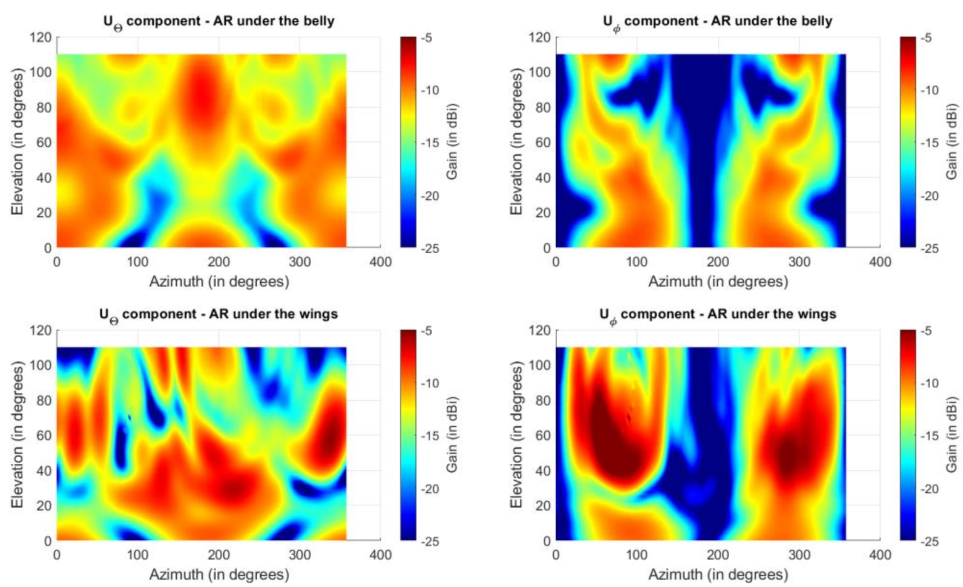

Figure 11: BBV2 gain patterns at 130 MHz. AR under the belly (upper figures); AR under the wings (lower figures).

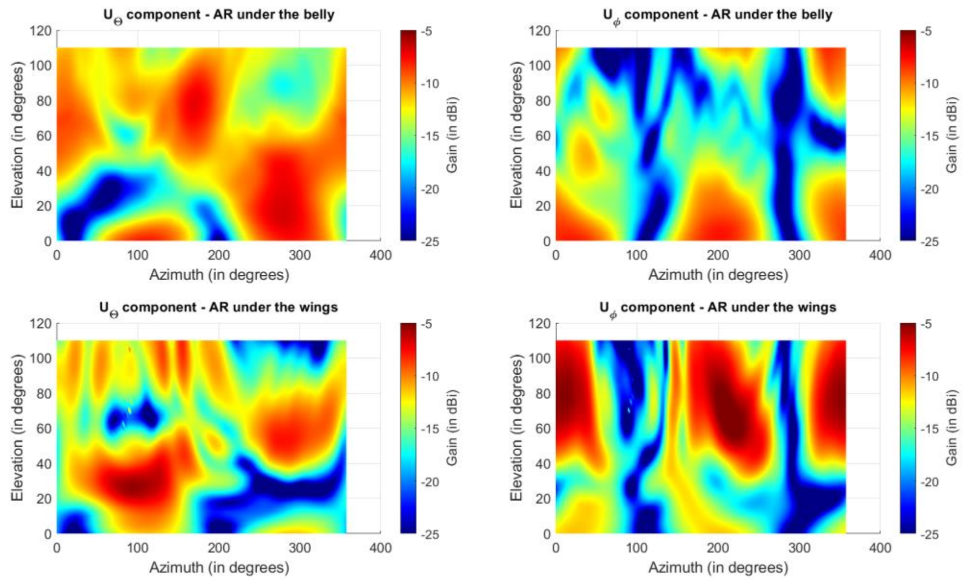

Figure 12: BBV3 gain patterns at 130 MHz. AR under the belly (upper figures); AR under the wings (lower figures).

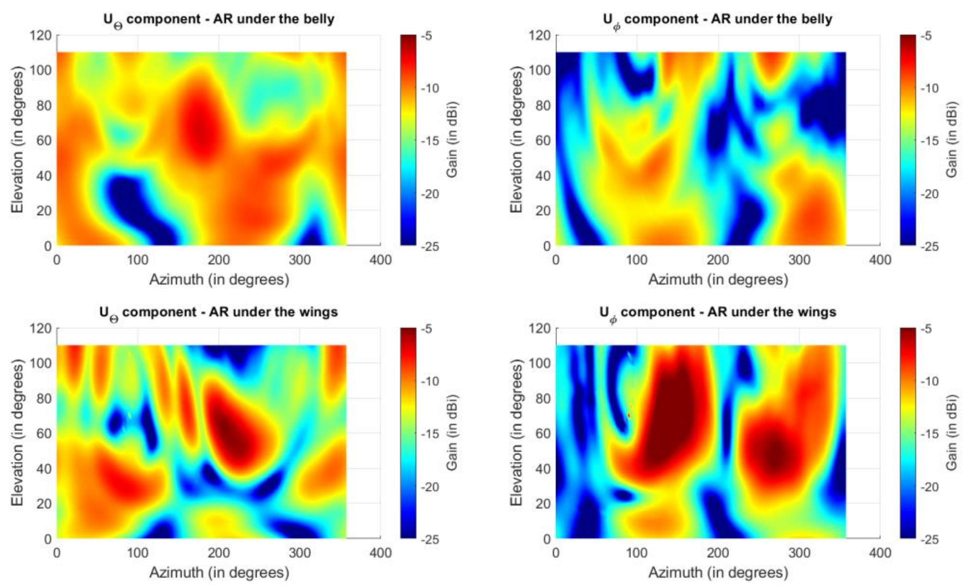

Figure 13: BBV4 gain patterns at 130 MHz. AR under the belly (upper figures); AR under the wings (lower figures).

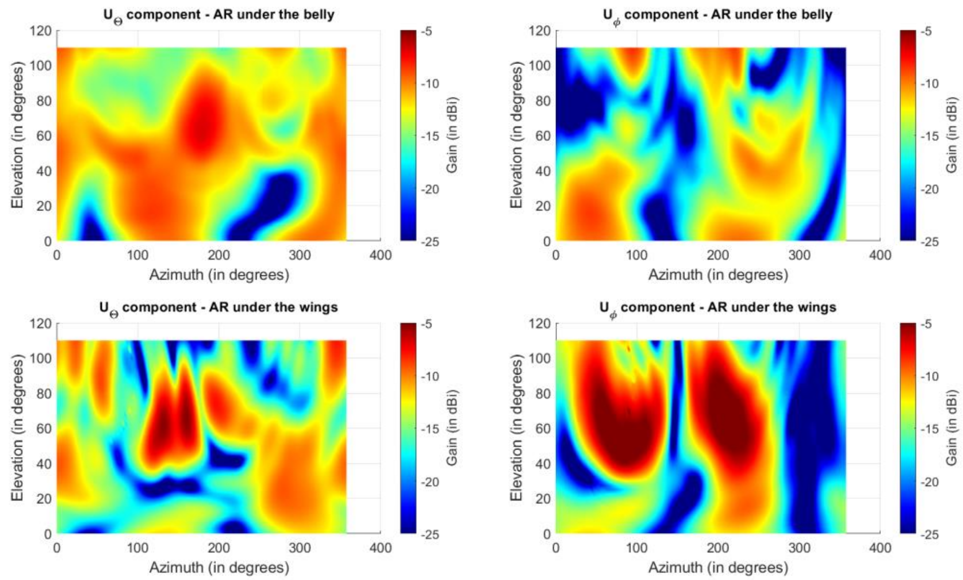

Figure 14: BBV5 gain patterns at 130 MHz. AR under the belly (upper figures); AR under the wings (lower figures).

4.3.1.3. 420 MHz

The figure 15 plots the BBV1 gain patterns (on E_θ and E_ϕ component) at 420 MHz. As previously, **we notice an important difference between gain patterns following the AR positions on the aircraft**. Moreover, the presence of the aircraft fuselage does not generate a significant masking area. Nevertheless, the aircraft fuselage induces some ripples due to multipath effects.

The same observations are valid on the other antennas: BBV5 (see figure 16), BBH1 (see figure 17) and BBH5 (see figure 18).

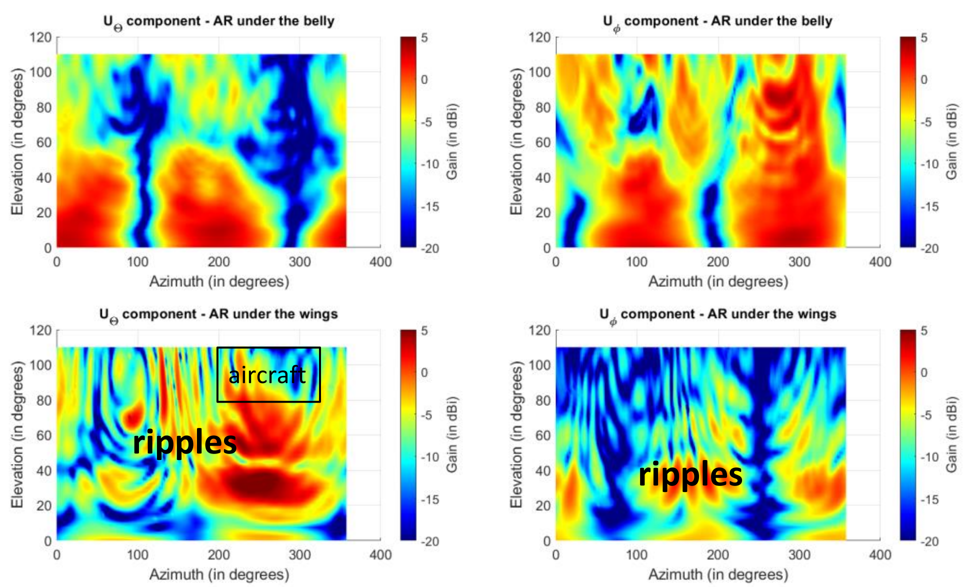

Figure 15: BBV1 gain patterns at 420 MHz. AR under the belly (upper figures); AR under the wings (lower figures).

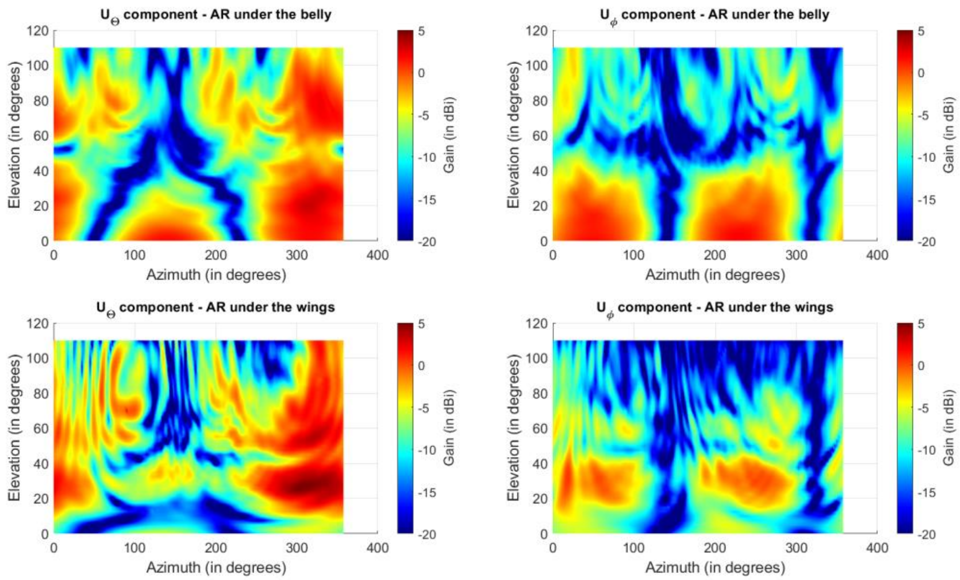

Figure 16: BBV5 gain patterns at 420 MHz. AR under the belly (upper figures); AR under the wings (lower figures).

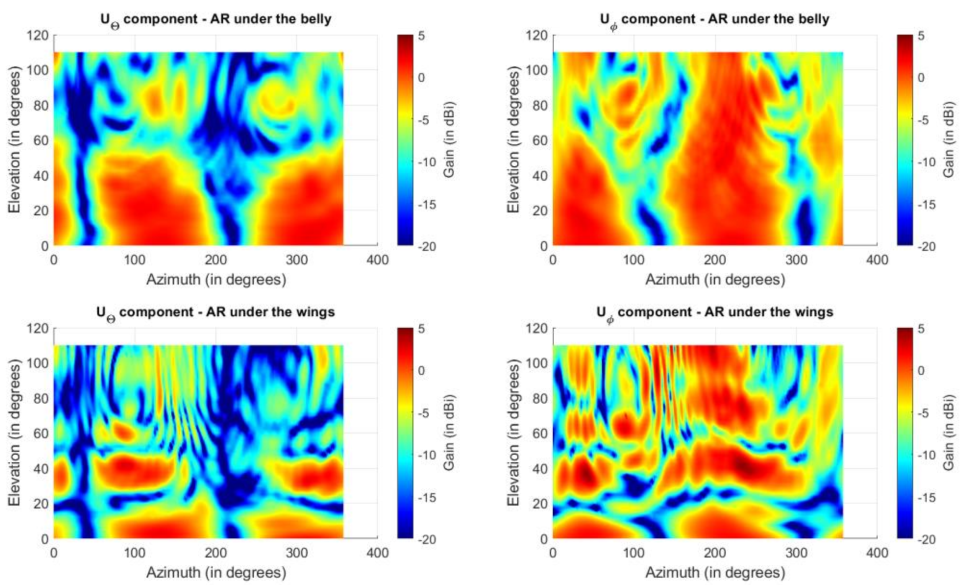

Figure 17: BBH1 gain patterns at 420 MHz. AR under the belly (upper figures); AR under the wings (lower figures).

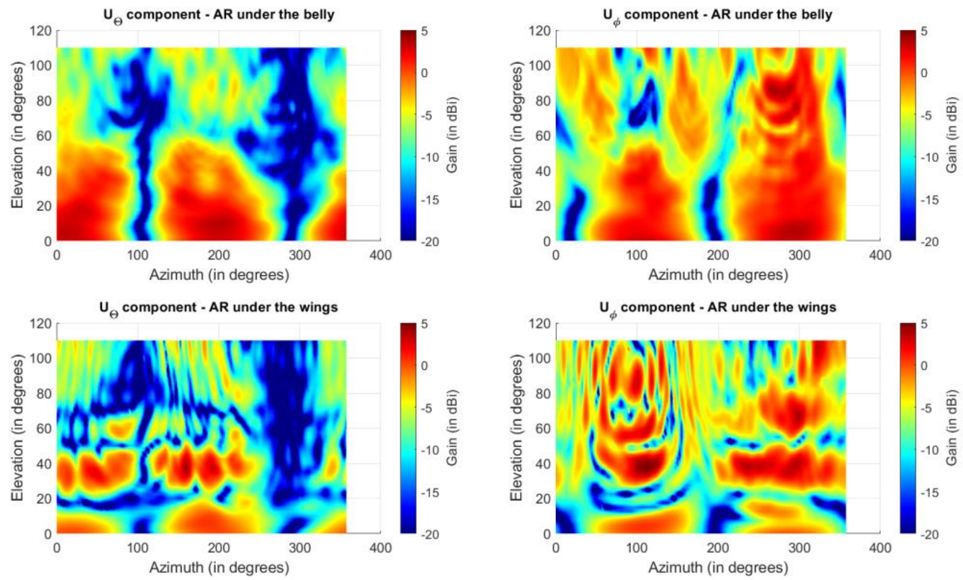

Figure 18: BBH5 gain patterns at 420 MHz. AR under the belly (upper figures); AR under the wings (lower figures).

4.3.1.4. 750 MHz

The figure 19 plots the BBV1 gain patterns (on E_θ and E_ϕ component) at 750 MHz. As previously, **we notice an important difference between gain patterns following the AR positions on the aircraft** (fewer differences on E_θ component). Moreover, the presence of the aircraft fuselage does not generate a significant masking area. Nevertheless, the aircraft fuselage induces some ripples due to multipath effects.

The same observations are valid on the other antennas: BBV5 (see figure 20), BBH1 (see figure 21) and BBH5 (see figure 22).

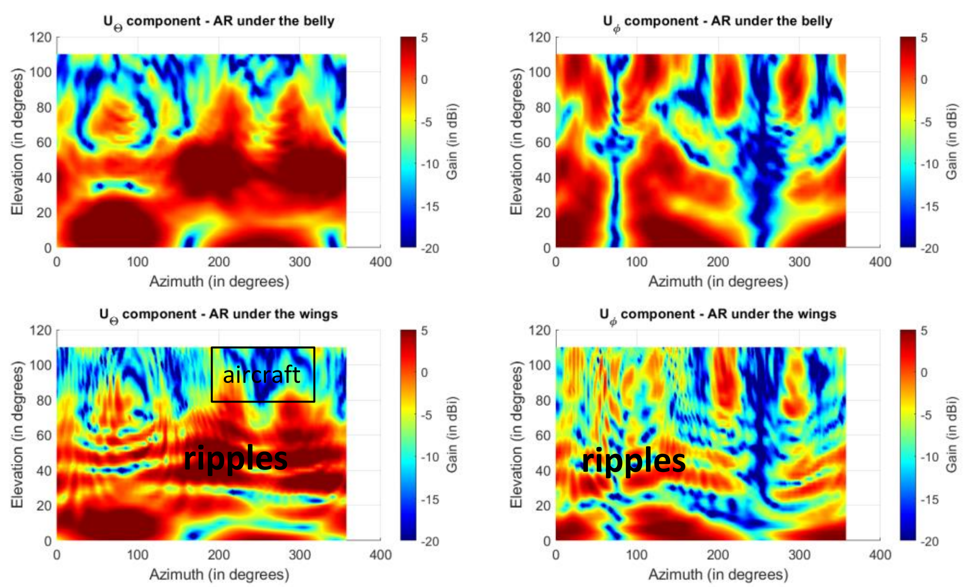

Figure 19: BBV1 gain patterns at 750 MHz. AR under the belly (upper figures); AR under the wings (lower figures).

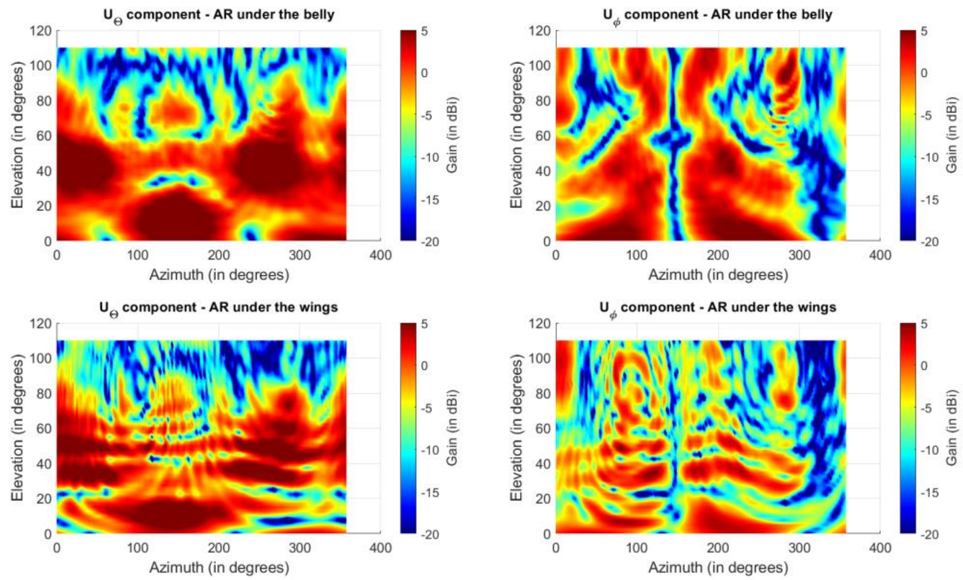

Figure 20: BBV5 gain patterns at 750 MHz. AR under the belly (upper figures); AR under the wings (lower figures).

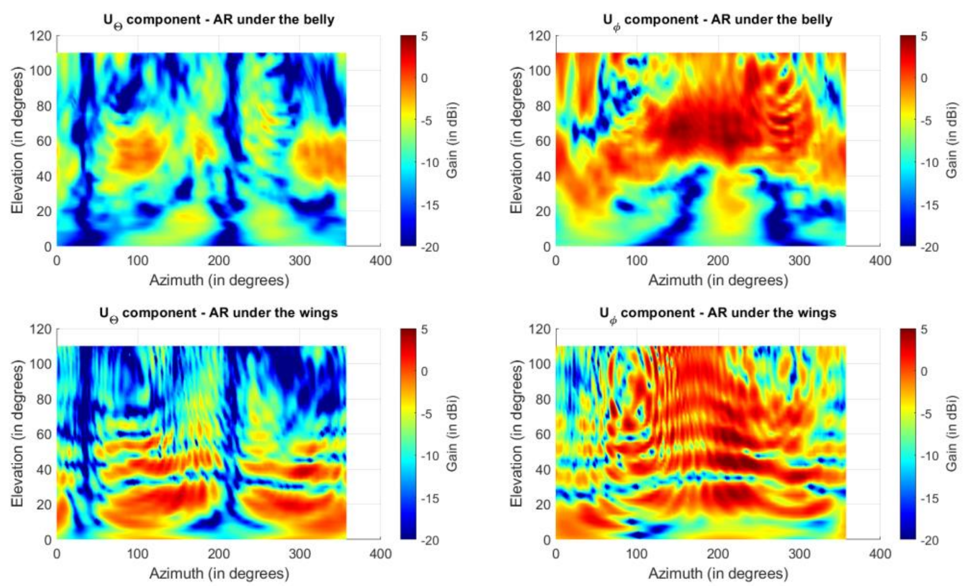

Figure 21: BBH1 gain patterns at 750 MHz. AR under the belly (upper figures); AR under the wings (lower figures).

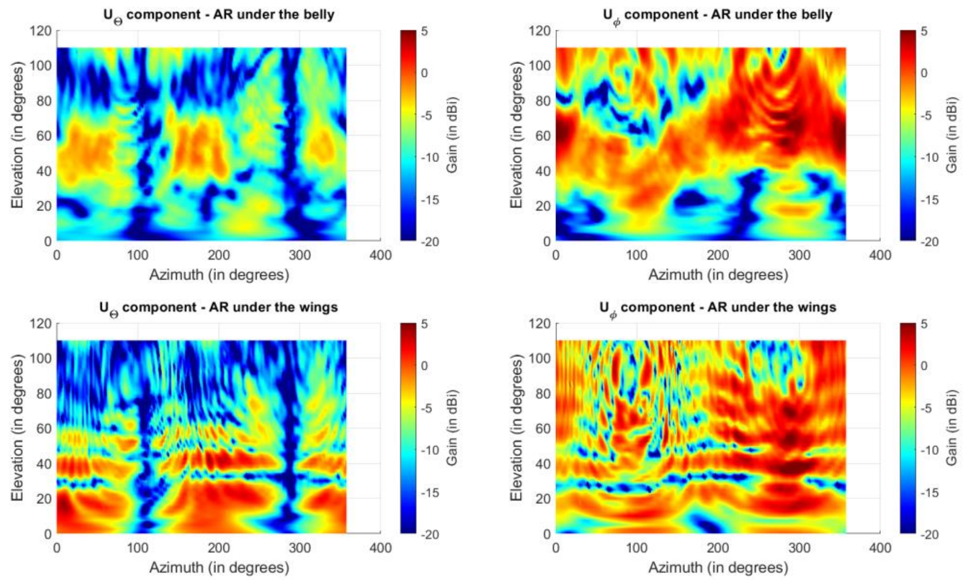

Figure 22: BBH5 gain patterns at 750 MHz. AR under the belly (upper figures); AR under the wings (lower figures).

4.3.2. In high band (764-3000 MHz)

To illustrate the influence of the BN2 Islander on the AR radiation patterns, some cartographies at different frequencies (800 MHz, 1640 MHz, 2640 MHz) are given in the following figures. The first and last frequencies correspond to cellular frequencies (B20 DL and B7 DL). The second one is in satellite phone band.

First, the antennas position in the coordinate system is given in the following figure 4 23.

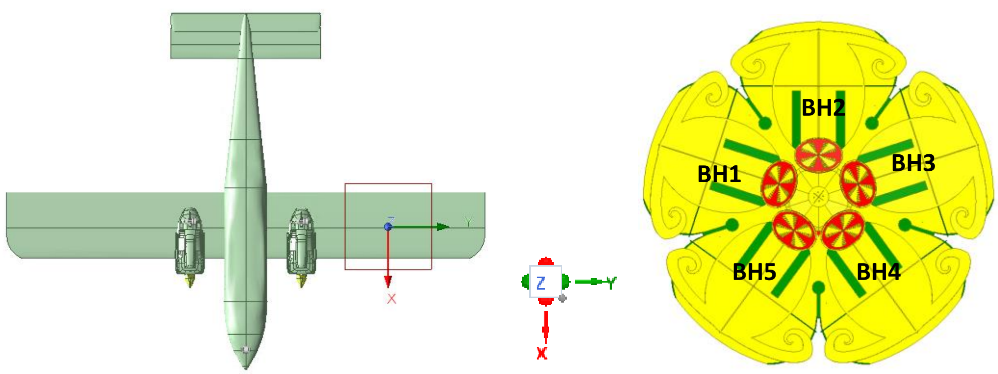

Figure 23: Antennas position in the coordinate system.

4.3.2.1. 800 MHz

The figure 25 plots the BH1P gain patterns (on E_θ and E_ϕ component) at 800 MHz. The figure compares the gain patterns for two different AR configurations:

- AR alone (in the two top cartographies): correspond to the high band calibration realized in anechoic chamber,
- AR under the wings (in the two lower cartographies).

As illustrated, for the two components of the E-field, the gain patterns are quite similar following the AR configurations. Nevertheless, some ripples are noticed due to multipath effects (destructive or constructive reflections on the aircraft fuselage). To illustrate the phenomenon (see figure 24), the gain (on E_θ component) of the antenna BH1P is plotted on two cut-planes (Azimuth=20° a. and Azimuth=200° b.).

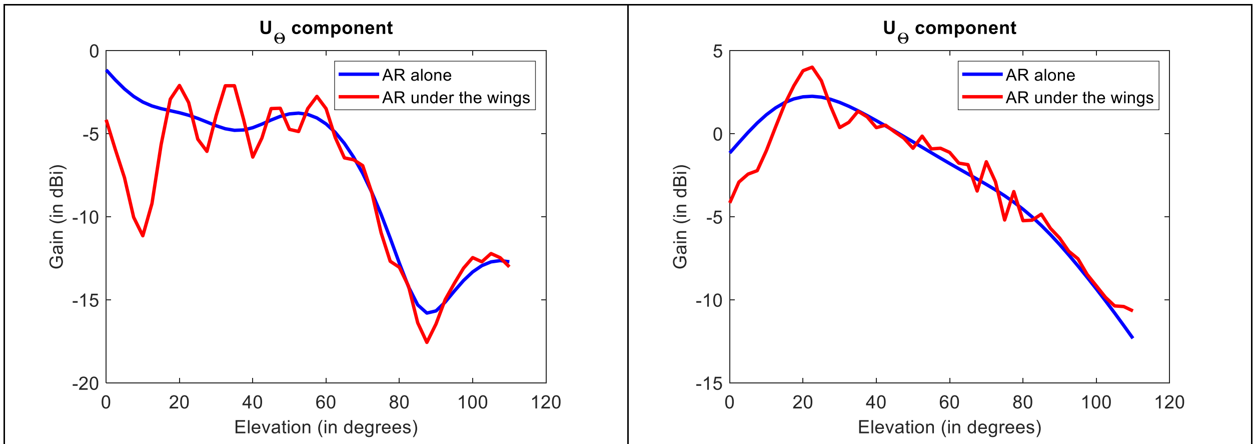

a.	*b.*

Figure 24: BH1P gain in two cut-planes: Azimuth=20° a.; Azimuth=200° b.

Furthermore, at this frequency, we can also note a limited masking area due to the aircraft fuselage.

The same observations are valid on the other antennas: BH5P (see figure 26), BH1M (see figure 27) and BH5M (see figure 28).

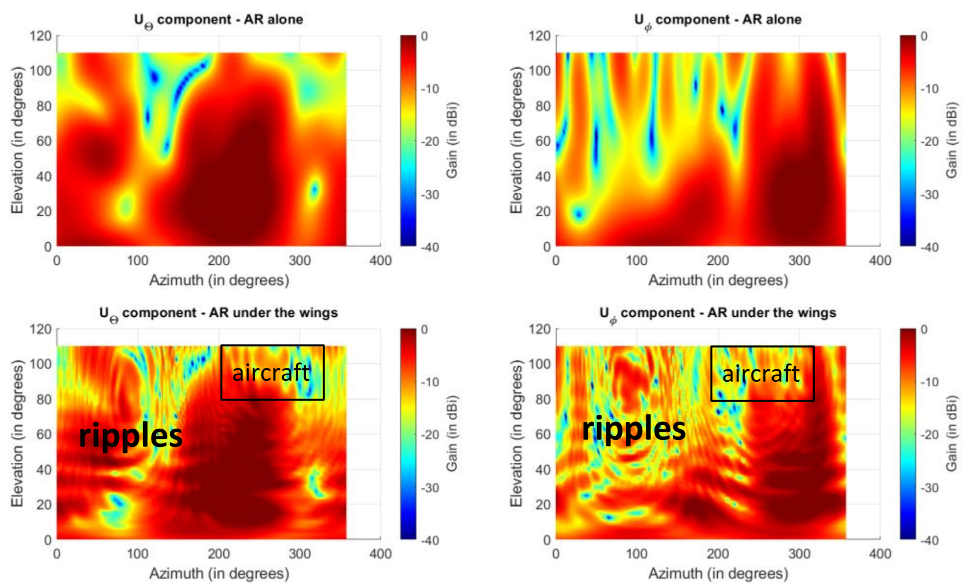

Figure 25: BH1P gain patterns at 800 MHz. AR alone (upper figures); AR under the wings (lower figures).

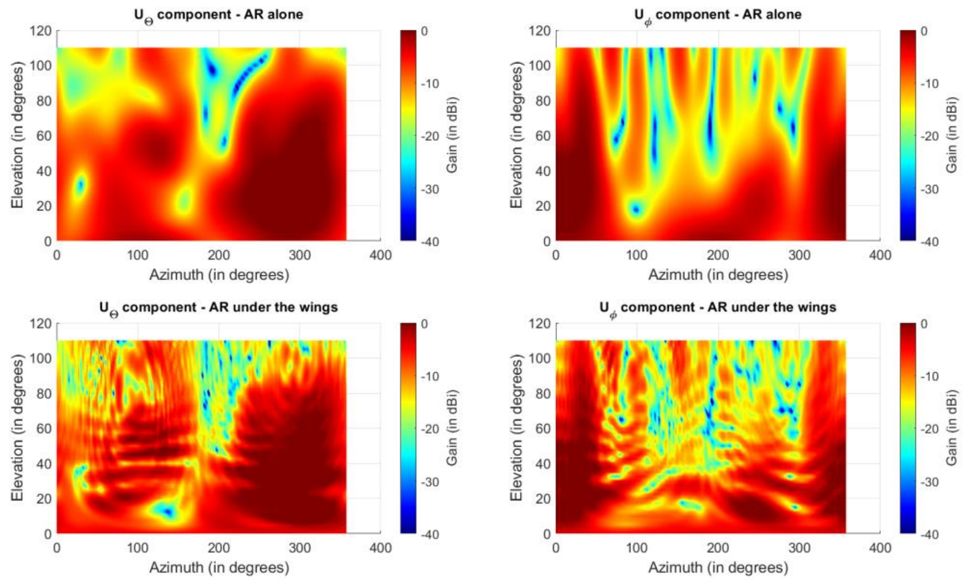

Figure 26: BH5P gain patterns at 800 MHz. AR alone (upper figures); AR under the wings (lower figures).

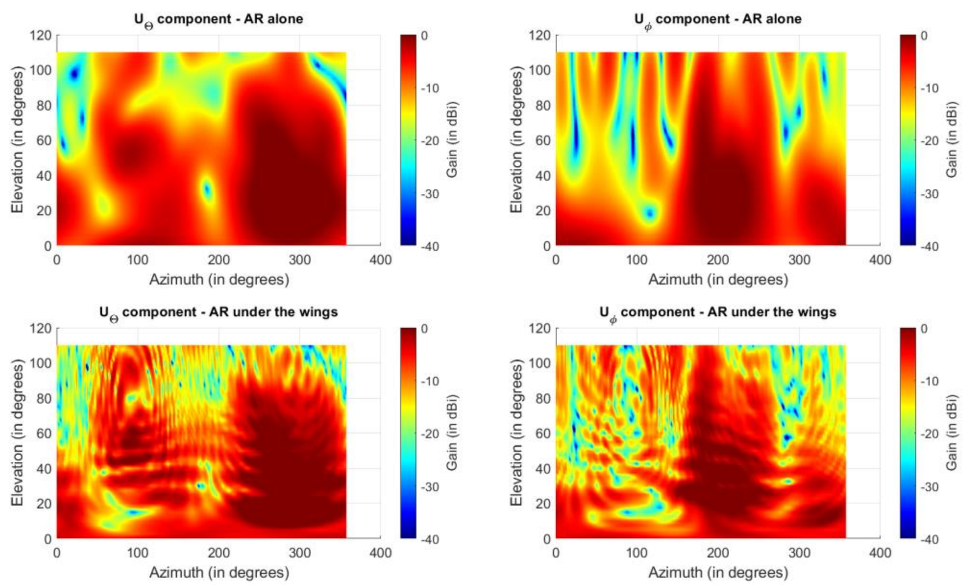

Figure 27: BH1M gain patterns at 800 MHz. AR alone (upper figures); AR under the wings (lower figures).

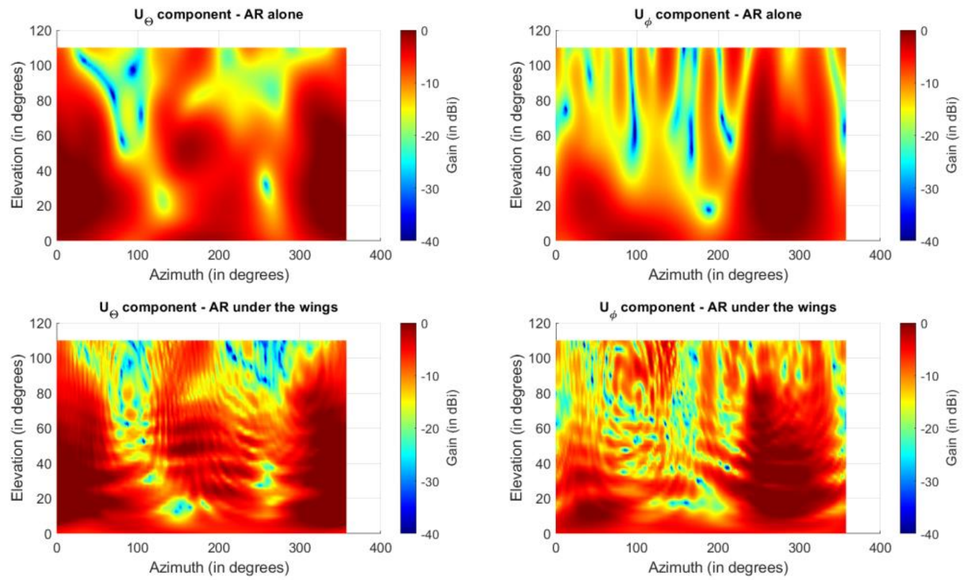

Figure 28: BH5M gain patterns at 800 MHz. AR alone (upper figures); AR under the wings (lower figures).

4.3.2.2. 1640 MHz

The figure 30 plots the BH1P gain patterns (on E_θ and E_ϕ component) at 1640 MHz. As previously, we notice very limited differences between gain patterns following the AR configurations (alone or under the wings). **Furthermore, the ripples observed when the AR is under the wings are less important compared to 800 MHz.**

To illustrate this (see figure 29), the gain of the antenna BH1P is plotted on two different cut-planes (Azimuth=20° a. and Azimuth=200° b.) following the two configurations.

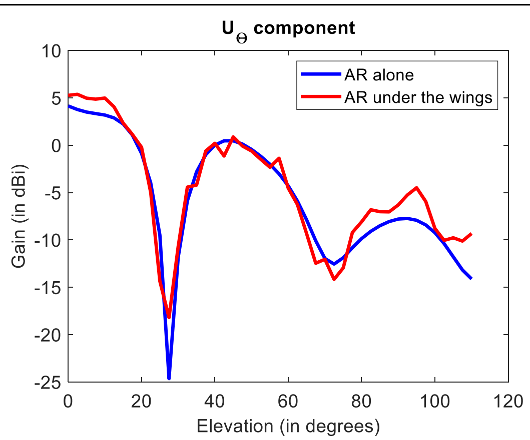	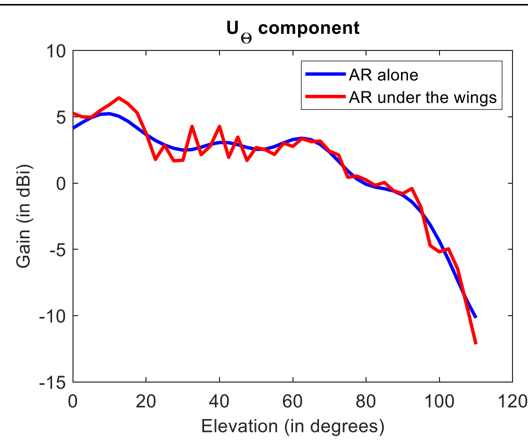
a.	***b.***

Figure 29: BH1P gain in two cut-planes: Azimuth=20° a.; Azimuth=200° b.

Furthermore, at this frequency, we can also note a limited masking area due to the aircraft fuselage.

The same observations are valid on the other antennas: BH5P (see figure 31), BH1M (see figure 32) and BH5M (see figure 33).

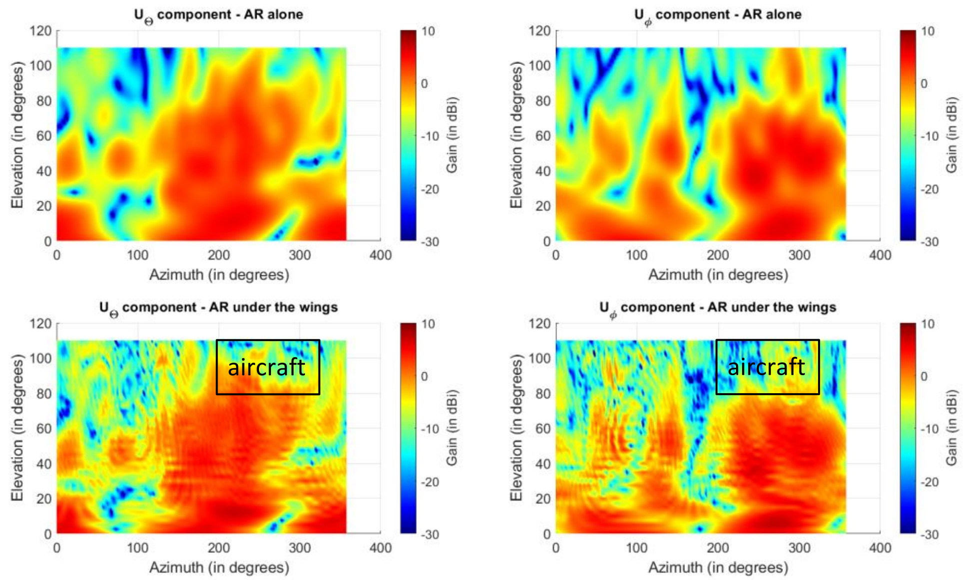

Figure 30: BH1P gain patterns at 1640 MHz. AR alone (upper figures); AR under the wings (lower figures).

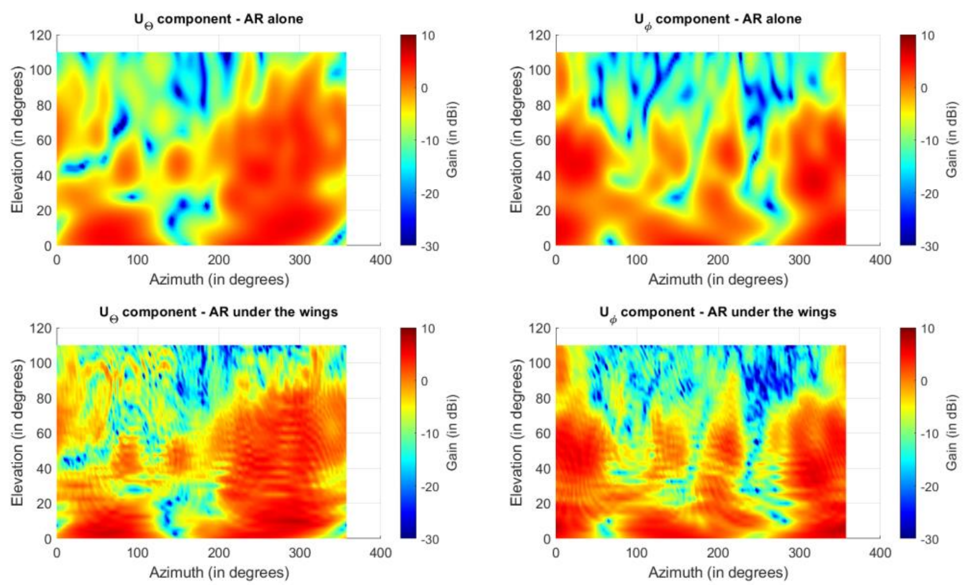

Figure 31: BH5P gain patterns at 1640 MHz. AR alone (upper figures); AR under the wings (lower figures).

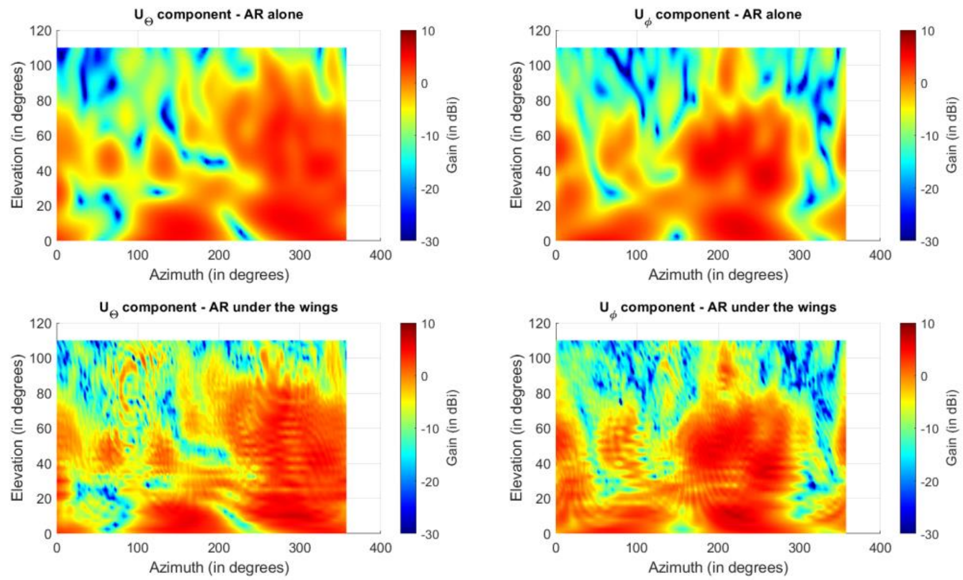

Figure 32: BH1M gain patterns at 1640 MHz. AR alone (upper figures); AR under the wings (lower figures).

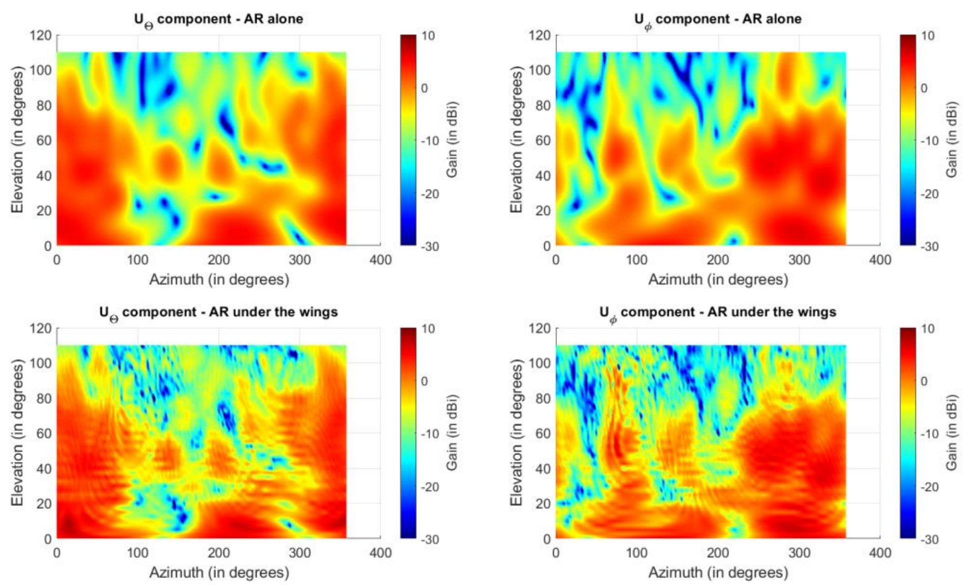

Figure 33: BH5M gain patterns at 1640 MHz. AR alone (upper figures); AR under the wings (lower figures).

4.3.2.3. 2640 MHz

The figure 35 plots the BH1P gain patterns (on E_θ and E_ϕ component) at 2640 MHz. As previously, **we notice very limited differences between gain patterns following the AR configurations (alone or under the wings).** Furthermore, the ripples observed when the AR is under the wings are less important compared to previous analysed frequencies (800 MHz and 1640 MHz). To illustrate this (see figure 34), the gain of the antenna BH1P is plotted on two different cut-planes (Azimuth=50° a. and Azimuth=200° b.) following the two configurations.

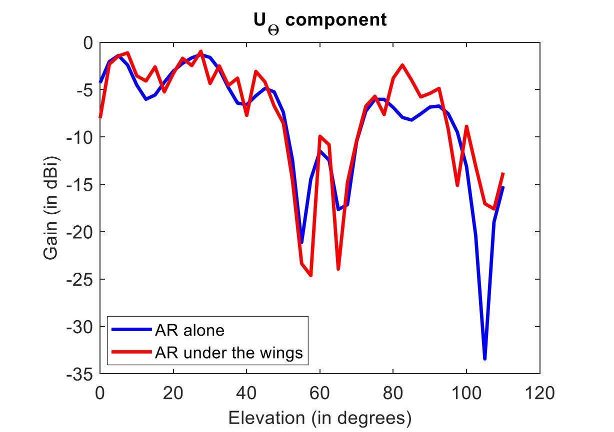	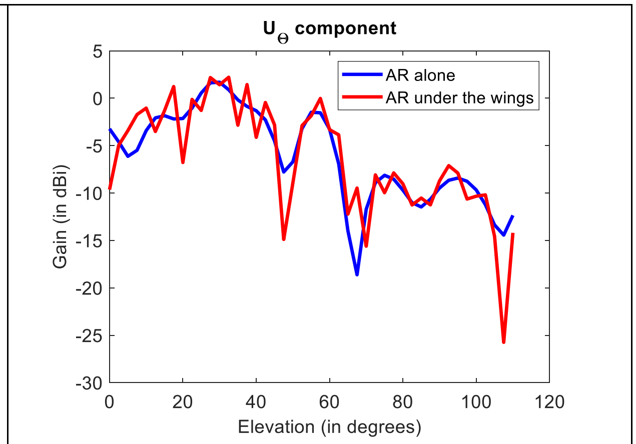
a.	***b.***

Figure 34: BH1P gain in two cut-planes: Azimuth=50° a.; Azimuth=200° b.

Furthermore, at this frequency, we can also note a limited masking area due to the aircraft fuselage.

The same observations are valid on the other antennas: BH5P (see figure 36), BH1M (see figure 37) and BH5M (see figure 38).

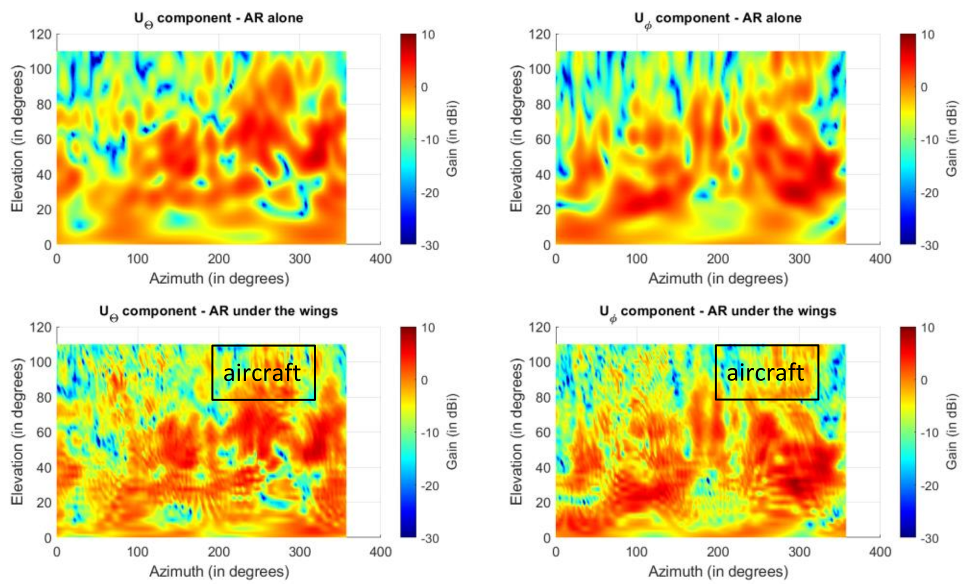

Figure 35: BH1P gain patterns at 2640 MHz. AR alone (upper figures); AR under the wings (lower figures).

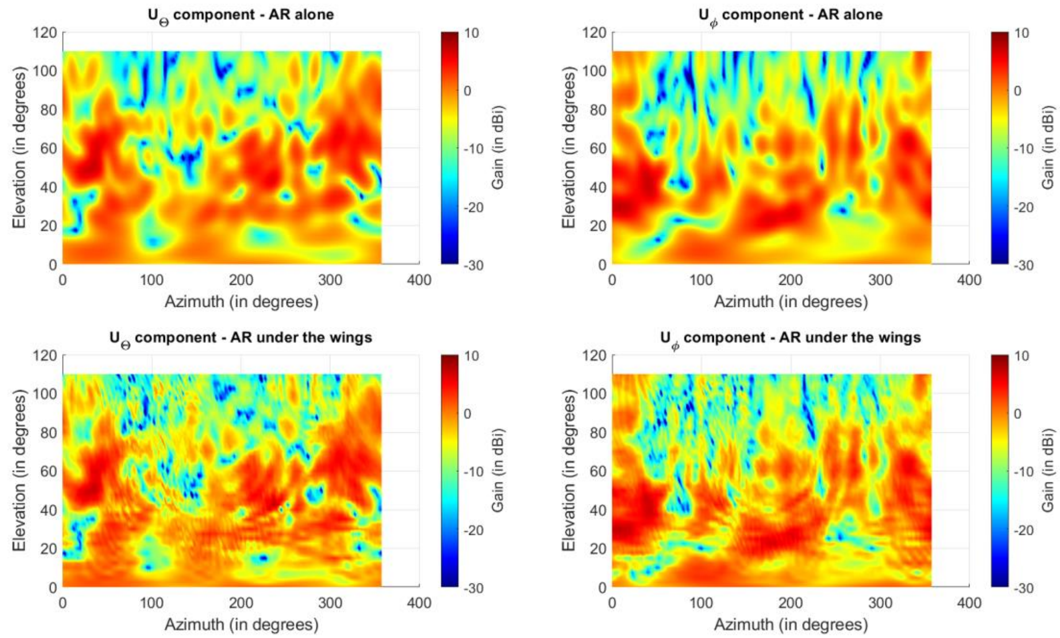

Figure 36: BH5P gain patterns at 2640 MHz. AR alone (upper figures); AR under the wings (lower figures).

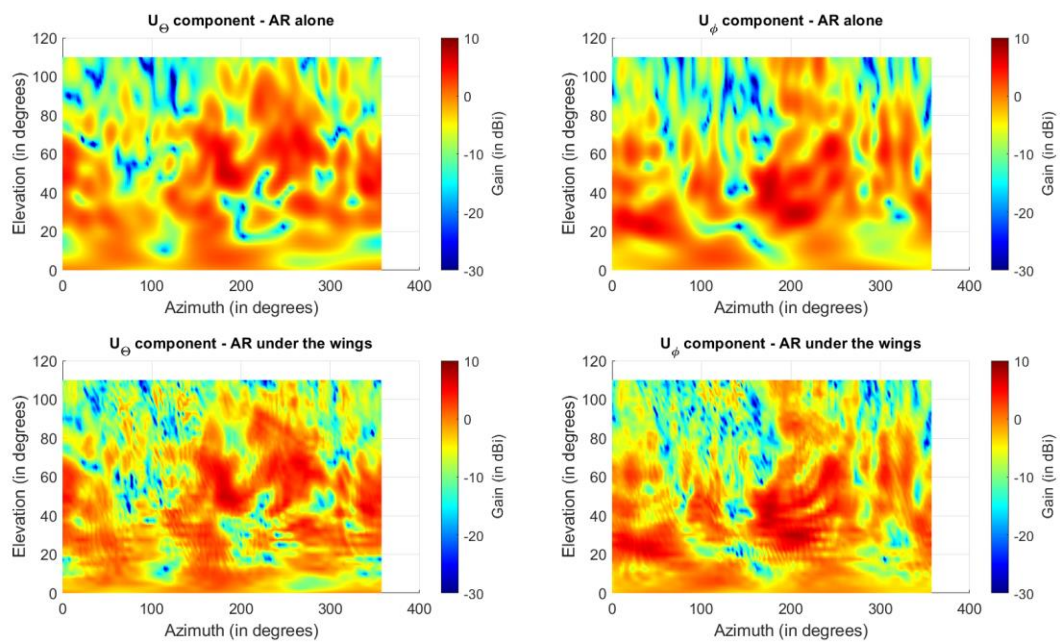

Figure 37: BH1M gain patterns at 2640 MHz. AR alone (upper figures); AR under the wings (lower figures).

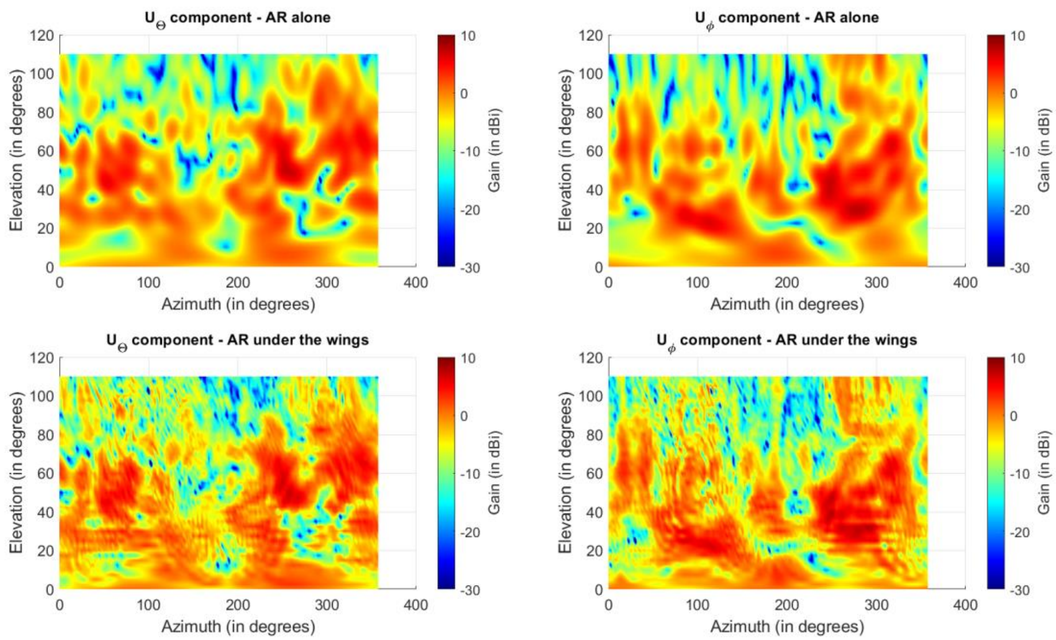

Figure 38: BH5M gain patterns at 2640 MHz. AR alone (upper figures); AR under the wings (lower figures).

4.3.3. CONCLUSIONS

This chapter analyses the influence of the AR placement on the radiation patterns performances. We can divide the conclusions following the AR sub-bands:

In low band (30-764 MHz):

- Due to antenna placement, the masking area is limited,
- Ripples appear in high frequencies due to multipath effects : this phenomenon can reduce locally the system sensitivity,
- Radiation patterns are significantly different when the AR is positioned under the belly or under the wings. Nevertheless, the low band is calibrated on aircraft.

In High band (764-3000 MHz):

- Due to antenna placement, the masking area is limited,
- Ripples (more important in low frequencies) appear when the AR is placed on the aircraft,
- Usually, the high band is not calibrated on aircraft. Thus, **it is necessary to estimate the localization degradation when the AR is placed under the wing compared to the usual integration (under the belly).** A tool has been developed to quantify the complex radiation pattern (amplitude and phase) modification between the calibrated AR configuration (alone in an anechoic chamber) and integrated on the aircraft (under the wing in our case). This tool is a mathematical function called “correlation” (used in image processing). The function (corr2) computes the correlation coefficient using:

$$r = \frac{\sum_m \sum_n (A_{mn} - \overline{A})(B_{mn} - \overline{B})}{\sqrt{\left(\sum_m \sum_n (A_{mn} - \overline{A})^2\right)\left(\sum_m \sum_n (B_{mn} - \overline{B})^2\right)}}$$

Where $\bar{A}$ = mean2(A), and $\bar{B}$ = mean2(B). “mean2(A)” is the mean of all values in array A.

The function returns:

- $r = 1$: if the two matrixes (here cartographies) are the same,
- $r = 0$: if the two matrixes (here cartographies) are totally different.

Example 1:

Cartography A:

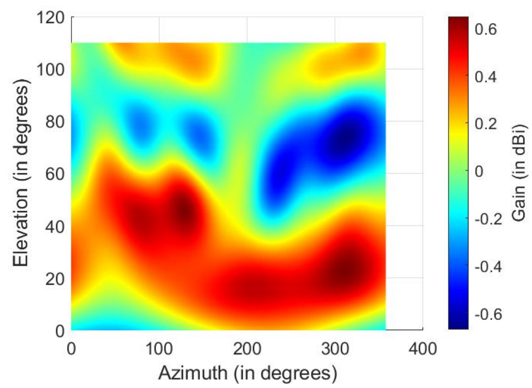

Cartography B:

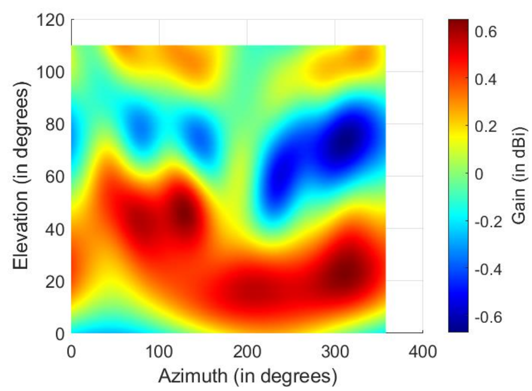

$r = 1$

Example 2:

Cartography A:

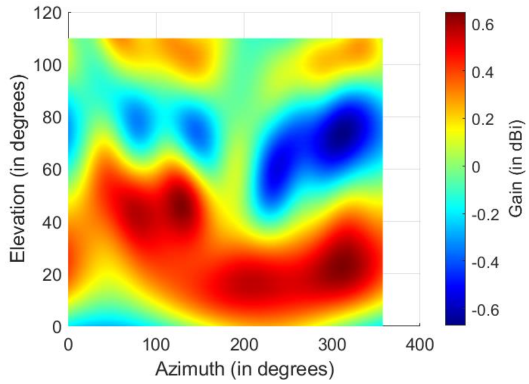

Cartography B:

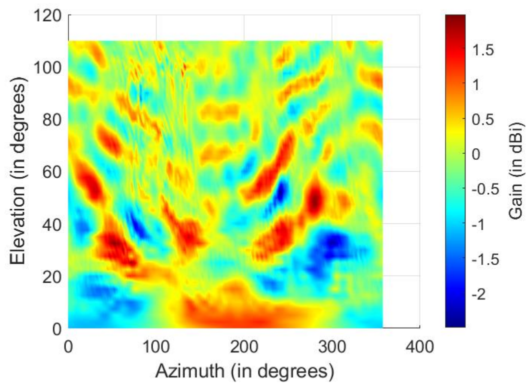

$r \approx 0.3$

Example 3:

Cartography A:

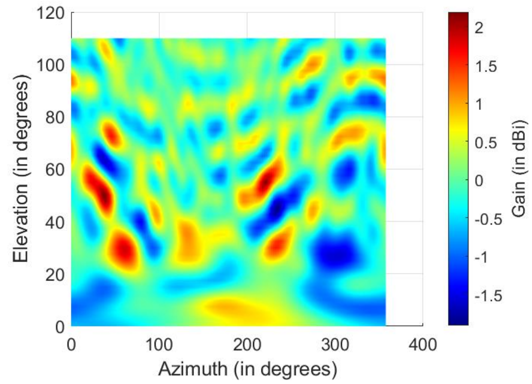

Cartography B:

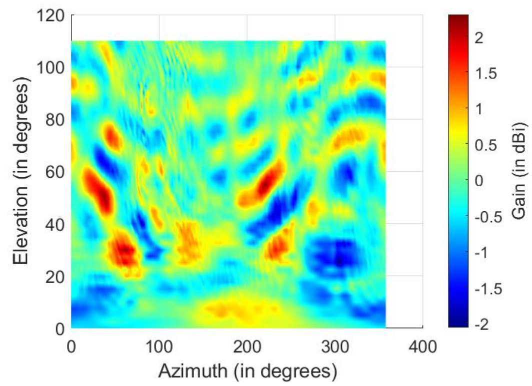

$r \approx 0.9$

Thus, the calculation was performed between the AR alone and the AR under the wing of the BN2 Islander. The results for 5 antennas (BH1P, BH2P, BH3P, BH4P and BH5P) are given in the following table 1.

We can note that the correlation is increasing with frequencies. At low frequencies, we can also notice that the worst correlation is obtained for BH1P antenna.

Referring to the figure 23, the BH1 antenna is looking towards the aircraft fuselage.

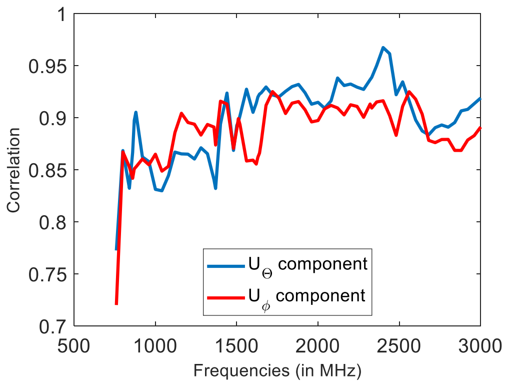

BH1P

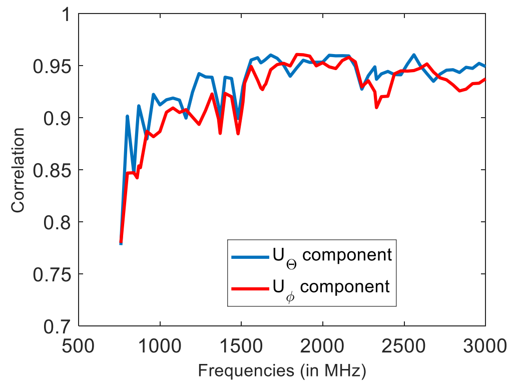

BH2P

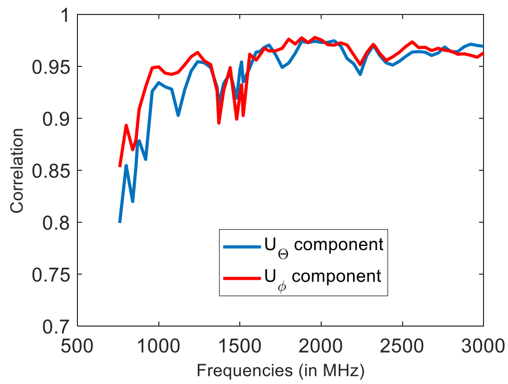

BH3P

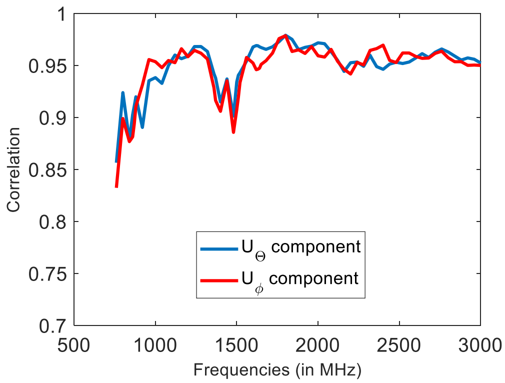

BH4P

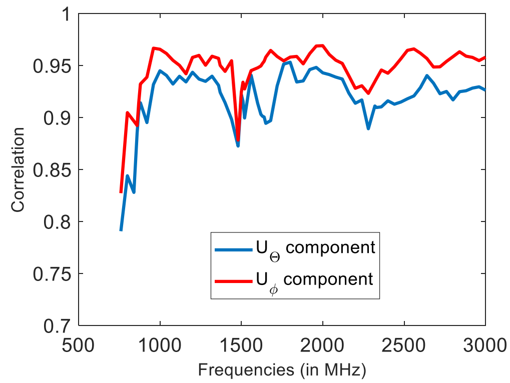

BH5P

Table 1: Correlation between AR alone and AR under a wing of BN2 Islander for 5 high band antennas.

This correlation function gives some indications on how the radiation patterns are modified by integration under the wing of a BN2 Islander aircraft.

In the next chapter, we analyse the localization degradation.

4.4. LOCALIZATION DEGRADATION

4.4.1. METHODOLOGY

The methodology used is described as follows:

1. Electromagnetic simulations of the AR alone. With these simulations, we generate a calibration table.
2. Then, we add noise (SNR=20 dB) to the electromagnetic simulation of the AR alone. According to the DoA algorithm, we can, thus, estimate the best achieved performances.
3. Then, we add noise (SNR= 20 dB) to the electromagnetic simulation of the AR integrated under the wing of BN2 Islander aircraft.
4. Finally, we compare the performances obtained in 2. and 3. in order to estimate the localization degradation.

4.4.2. RESULTS

For the methodology given previously, we calculate the localization error.

- With the AR alone (methodology 2., see figure 39 a.), the location error is lower than 2.5° on 760-3000 MHz frequency range. The localization error is lower than 1° for frequencies higher than 1300 MHz.
- With the AR under the wing of the BN2 Islander (methodology 3., see figure 39 b.), the localization error is higher than 2.5° for frequencies lower than 960 MHz. Furthermore, over the whole frequency range, the localization error is higher than 1°. As a result, we can estimate the localization degradation (methodology 4.) due to integration under the wing.

  As plotted in the figure 40, **the localization degradation is higher than 2.5° for frequencies lower than 900 MHz and close to 2° for frequencies higher than 1 GHz.**

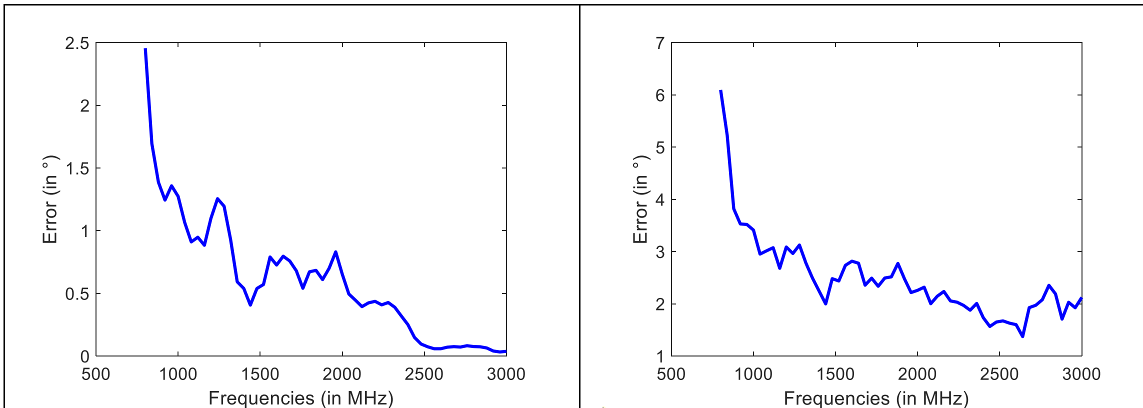

a.	***b.***

Figure 39: Localization performances with AR alone a. and AR under the wing b.

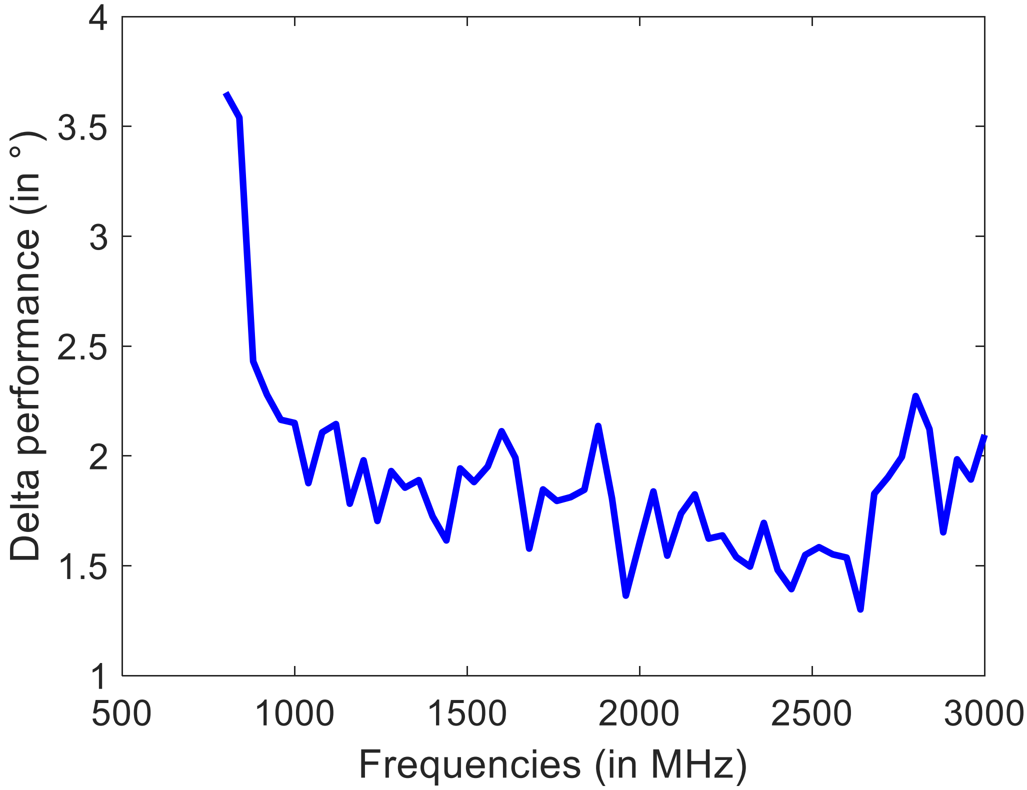

Figure 40: Localization degradation due to integration under the wing of BN2 Islander aircraft.

Considering the results and in order to ensure acceptable performances, it would be necessary to calibrate on the aircraft frequencies lower than 960 MHz (subject to the agreement of the authorities).

For frequencies higher than 960 MHz, the calibration done with AR alone in anechoic chamber is sufficient.

5. COUPLING BETWEEN ON BOARD EMITTERS AND THE ANTENNA ARRAY

5.1. ON BOARD EMITTERS

The emitters on INCAS BN2 Islander are as follows:

- Aircraft VHF radio GARMIN GNC255A: 118.000 to 136.992 MHz, 8.33 kHz channel spacing. 10W RF power.
- ELT – ARTEX C406-2: 406 MHz; 121,5 MHz.
- ATC Bendix-King KT76A: 1090Mhz #3Mhz, 200W peak power.
- DME Bendix-King KN 65: 108-117Mhz, 200W peak

The emitters positions are also given by INCAS (see figure 41 for a VHF radio):

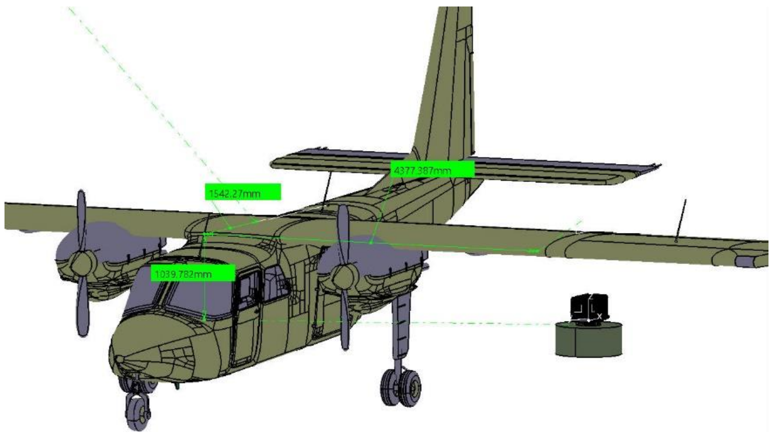

Figure 41: VHF radio position on INCAS BN2 Islander.

According to this information, some electromagnetic simulations (using SBR solver) were performed on the HFSS software (see figure 42).

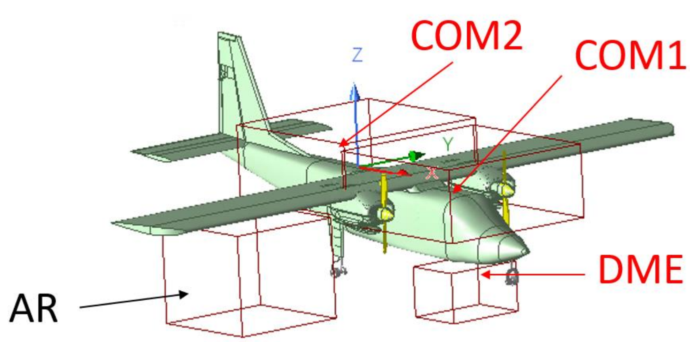

Figure 42: Coupling simulations between emitters and the AR (using SBR solver).

5.2. DESIGN OF TRANSMITTING ANTENNAS

Before simulating the emitters and the AR on the aircraft, it is necessary to design the transmitting antenna as close as possible to reality. The transmitting antennas have omnidirectional radiation patterns. Thus, blade antennas (see figure 43) have been chosen for the design of transmitting antennas (see figure 44 for the antenna radiation pattern). The antenna dimensions have been optimized for the different radios to operate at the correct frequency.

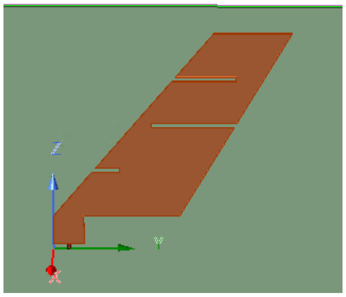

Figure 43: Blade antenna.

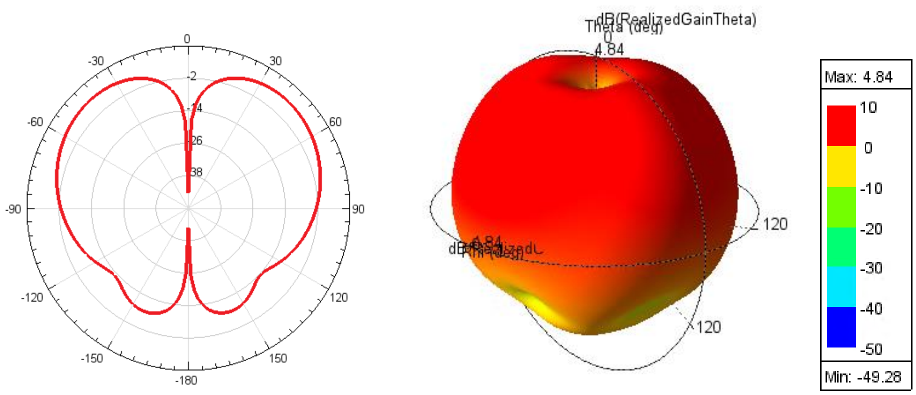

Figure 44: Blade antenna radiation pattern.

5.3. RESULTS

The following parts discuss the influence of each emitter on FlashHawk system. The study is divided into two parts:

- First, we check if the power radiated by each emitter can cause damage on FlashHawk.
- Then, we evaluate the impact on FlashHawk sensitivity.

5.3.1. COM1 EMITTER

In this part, we analyse the coupling between the COM1 emitter and the Antenna Array (see figure 45). As a reminder, the COM1 operates from 118 MHz to 136.992 MHz with 10W RF power.

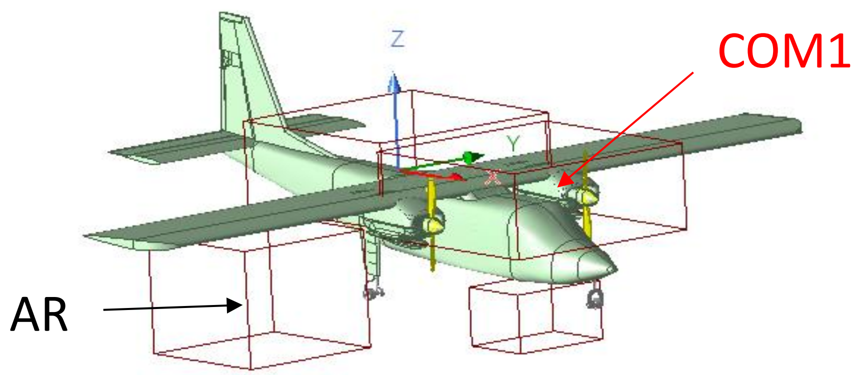

Figure 45: EM simulations of coupling between COM1 emitter and the AR.

The figure 46 plots the level on Antenna Array input (on calibration switch) with COM1 emissions. The EM simulations give the coupling between the emitter (COM1) and the 10 (low band here) antenna array ports. In the following figure, we plot the maximum coupling (for the 10 AR ports) between the emitter (COM1) and receiver (AR). As a result, the level on antenna input is between **-5 dBm and +2 dBm** over the whole frequency range of the COM1 radio. This level is around 15 dB lower than the limit to avoid damages on FlashHawk system.

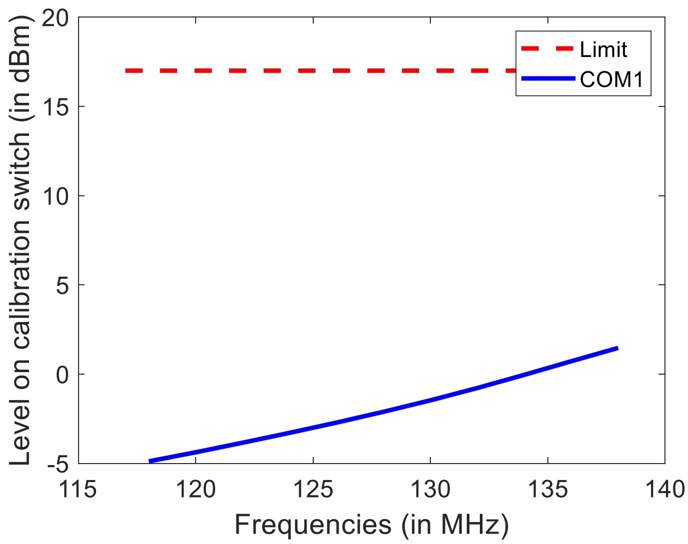

Figure 46: Level on antenna input (on calibration switch) versus frequencies for COM1 emitter and comparison with the limit to avoid damages on FlashHawk system.

The sensor RF front-end is divided in following sub-bands:

- 30-960 MHz,
- 960-1525 MHz,
- 1525-1680MHz,
- 1680-2300MHz,
- 2300-2690MHz,
- 2690-3000MHz.

Due to COM1 emissions, the FlashHawk performances is highly degraded in the first sub-band. Thanks to a high pass filter, FlashHawk will be functional for frequencies higher than 650 MHz. Nevertheless, in the 30-650 MHz band, the sensitivity degradation of the FlashHawk system is higher than 30dB.
For your information, **a 30dB sensitivity degradation corresponds to a reduction of reading range by a factor higher than 30.**

5.3.2. COM2 EMITTER

Similarly to the previous part, we analyse, here, the coupling between the COM2 emitter and the Antenna Array (see figure 47). As a reminder, the COM2 operates from 118 MHz to 136.992 MHz with 10W RF power.

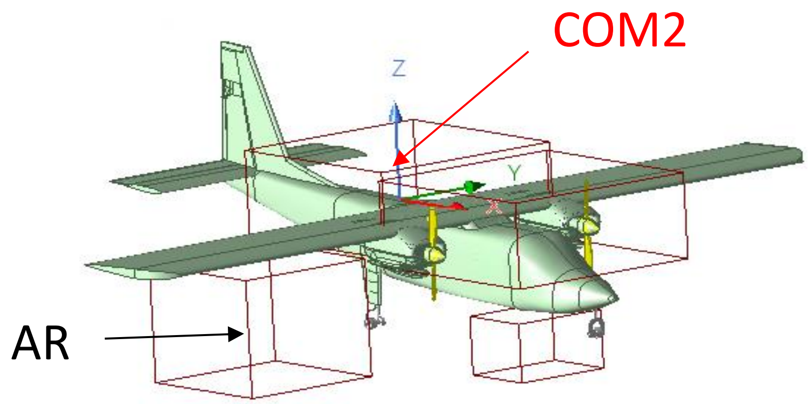

Figure 47: EM simulations of coupling between COM2 emitter and the AR.

The figure 48 plots the level on Antenna Array input (on calibration switch) with COM2 emissions. As a result, the level on antenna input is between **-5 dBm and 2 dBm** over the whole frequency range of the COM2 radio. This level is around 15 dB lower than the limit to avoid damages on FlashHawk system.

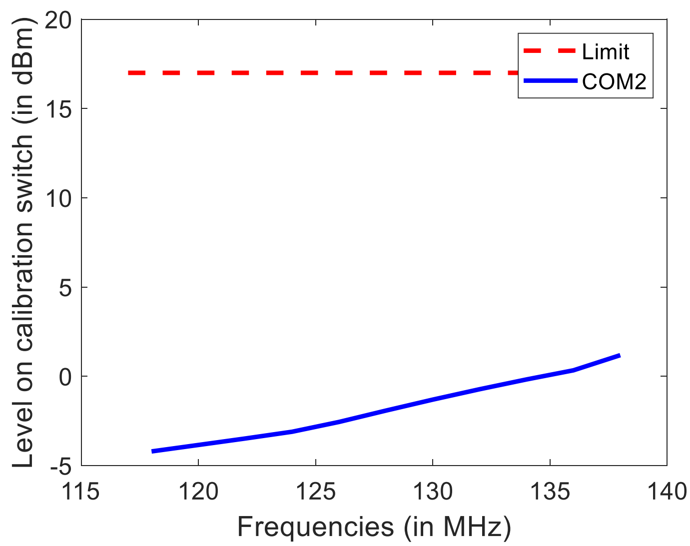

Figure 48: Level on antenna input (on calibration switch) versus frequencies for COM2 emitter and comparison with the limit to avoid damage on FlashHawk system.

Due to COM2 emissions, the FlashHawk performances is highly degraded in the sub-band: 30-650 MHz with a sensitivity degradation of the FlashHawk system is higher than 30dB.

5.3.3. DME Emitter

In this part, we analyse, here, the coupling between the DME emitter and the Antenna Array (see figure 4947). As a reminder, the DME operates from 108 MHz to 117 MHz with 200W RF peak power.

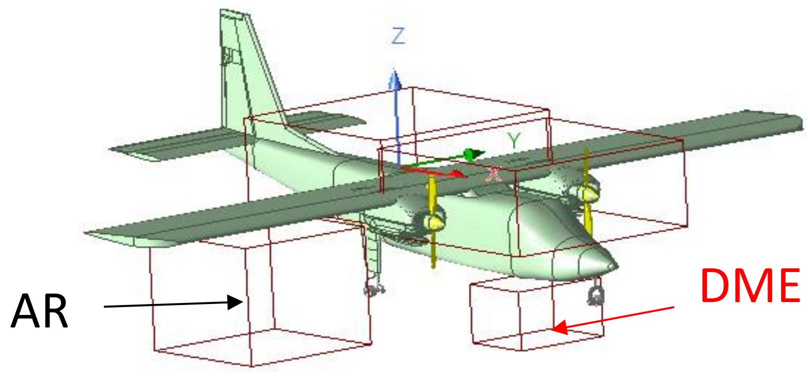

Figure 49: EM simulations of coupling between DME emitter and the AR.

The figure 5048 plots the level on Antenna Array input (on calibration switch) with DME emissions. As a result, the level on antenna input is between **8 dBm and 12 dBm** over the whole frequency range of the DME radio. This level is around 5 dB lower than the limit to avoid damages on FlashHawk system.

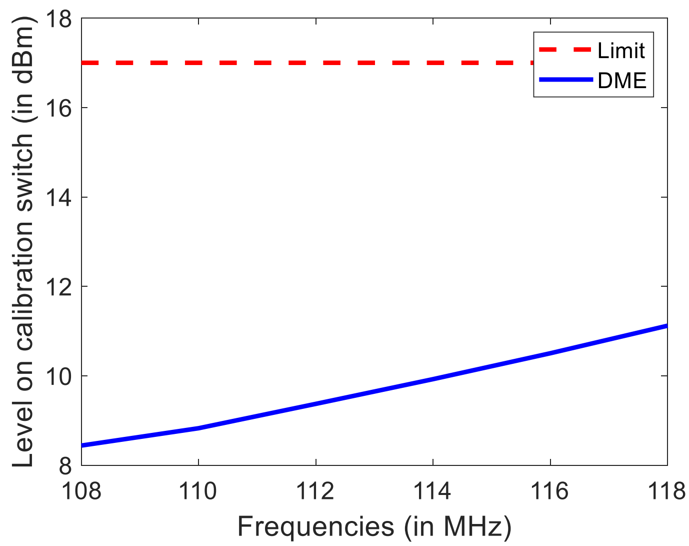

Figure 50: Level on antenna input (on calibration switch) versus frequencies for DME emitter and comparison with the limit to avoid damage on FlashHawk system.

Due to DME emissions, the FlashHawk performances is highly degraded in the sub-band: 30-650 MHz with a sensitivity degradation of the FlashHawk system is higher than 40dB.
For your information, **a 40dB sensitivity degradation corresponds to a reduction of reading range by a factor 100.**

5.3.4. ATC EMITTER

In this part, we analyse, here, the coupling between the ATC emitter and the Antenna Array (see figure 5147). As a reminder, the ATC operates at 1090 MHz with 200W RF peak power.

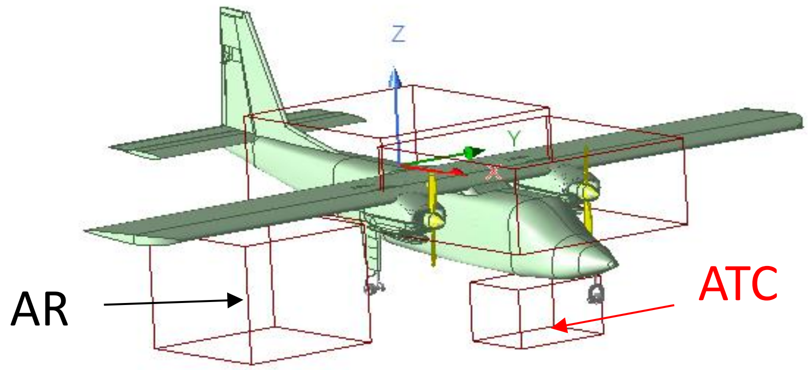

Figure 51: EM simulations of coupling between ATC emitter and the AR.

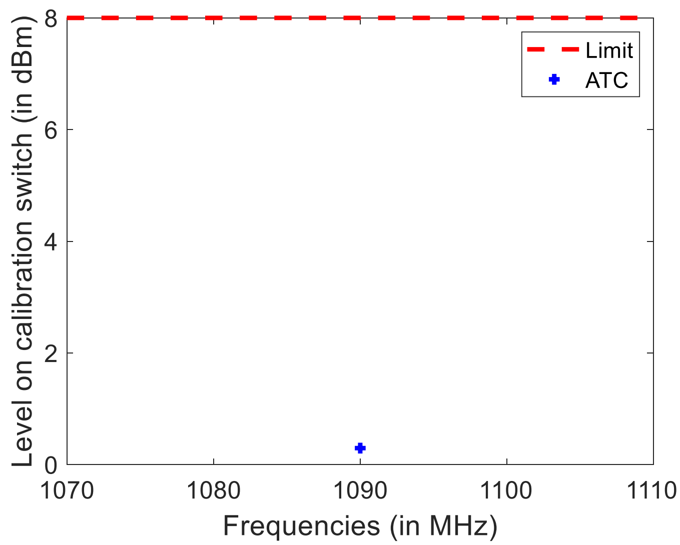

Figure 52: Level on antenna input (on calibration switch) versus frequencies for ATC emitter and comparison with the limit to avoid damage on FlashHawk system.

Due to ATC emissions, the FlashHawk performances is highly degraded in the sub-band: 960-1525 MHz with a sensitivity degradation of the FlashHawk system is higher than 30dB.

5.4. CONCLUSIONS

In this chapter, we analyze the impact of on-board emitters on FlashHawk performances. **The coupling between emitter (on-board radios) and receiver (Antenna Array),** obtained by EM simulations, **allows us to verify that there will be no damage on FlashHawk system.**

Nevertheless, **on-board emissions highly degrade the FlashHawk performances in several sub-bands.** The following table2 resumes the unusable frequency band according to the radio emissions.

For example, during ATC emissions, the sensor sub-band from 960 MHz to 1525 MHz is unusual. The other sub-bands are usable as usually.

	FlashHawk sub-bands						
On-board radio	30-650 MHz	650-960 MHz	960-1525 MHz	1525-1680 MHz	1680-2300 MHz	2300-2690 MHz	2690-3000 MHz
COM1 (118-136.992 MHz; 10 W)	✗	✓	✓	✓	✓	✓	✓
COM2 (118-136.992 MHz; 10 W)	✗	✓	✓	✓	✓	✓	✓
DME (108-117 MHz; 200 W)	✗	✓	✓	✓	✓	✓	✓
ATC (1090 MHz; 200 W)	✓	✓	✗	✓	✓	✓	✓

Table 2: Unusable sub-bands due to on-boards emissions.

6. CONCLUSIONS

This document discusses about 3D simulation performed on the electromagnetic software HFSS from Ansys. In this report, the analysis is divided into two parts:

- First, we analyze the influence of the BN2 Islander on AR performances. In the AR low band (30-764 MHz), we observe:
    - Due to antenna placement, the masking area is limited,
    - Ripples appear in high frequencies due to multipath effects : this phenomenon can reduce locally the system sensitivity,
    - Radiation patterns are significantly different when the AR is positioned under the belly or under the wings. Nevertheless, the low band is calibrated on aircraft.

  In the AR high band (764-3000 MHz), we notice:
    - Due to antenna placement, the masking area is limited,
    - Ripples (more important in low frequencies) appear when the AR is placed on the aircraft,
    - Considering the radiation patterns modifications on the aircraft and in order to ensure acceptable performances :
        - **it would be necessary to calibrate on the aircraft frequencies lower than 960 MHz (subject to the authorities agreement).**
        - **for frequencies higher than 960 MHz, the calibration done with AR alone in anechoic chamber is sufficient.**

  Furthermore, the movement at wing tip can reach a max of 30cm displacement (+/- 15 cm from neutral point). By considering a linear variation, **the wing movement induces a roll error of about 1.5°.**

  The following table synthesises the FlashHawk accuracy, after 5 seconds of interception and for elevation angle lower than -30°, for different AR positions and configurations:

		Frequency bands			
		30-100 MHz (Low band AR)	**100-760 MHz (Low band AR)**	**760-960 MHz (High band AR)**	**960-3000 MHz (High band AR)**
Configurations	**AR under belly without** aircraft calibration	**N/A***	**N/A***	**< 7°**	**< 7°**
	AR under the belly with aircraft calibration	**< 14°**	**< 7°**	**< 7°**	**< 7°**
	AR under the wings without aircraft calibration	**N/A***	**N/A***	< 7° + 4° (multipath effects) + 1.5° (wing movement): **< 12.5 °**	< 7° + 2.5° (multipath effects) + 1.5° (wing movement): **< 11 °**
	AR under the wings with aircraft calibration	< 14° + 1.5° (wing movement): **< 15.5°**	**< 7°** + 1.5° (wing movement): **< 8.5°**	**< 7°** + 1.5° (wing movement): **< 8.5°**	< 7° + 2.5° (multipath effects) + 1.5° (wing movement): **< 11 °**

* N/A: FlashHawk cannot be used.

- Then, we analyze the impact of on-board emitters on FlashHawk performances. **The coupling between emitter (on-board radios) and receiver (Antenna Array) allows us to check that there will be no damage on FlashHawk system.**

  Nevertheless, **on-board emissions highly degrade the FlashHawk performances in several sub-bands** (see table2 for full description of disturbed bandwidths). This limitation must be taken into account by operators.